

1

# **The role of *polycystic kidney disease-like* homologs in planarian nervous system regeneration and function**

4

5 Kelly G. Ross<sup>1</sup>, Sarai Alvarez Zepeda<sup>1</sup>, Mohammad A. Auwal<sup>1</sup>, Audrey K. Garces<sup>1</sup>,  
6 Sydney Roman<sup>1</sup>, and Ricardo M. Zayas<sup>1\*</sup>

<sup>7</sup> <sup>8</sup> <sup>1</sup>Department of Biology, San Diego State University, 5500 Campanile Dr., San Diego, CA 92182-4614, USA

9

## 10 \*Correspondence:

11

12 Ricardo M. Zayas

13 E-mail: [rzayas@sdsu.edu](mailto:rzayas@sdsu.edu)

14

15

## Abstract

16 Planarians are an excellent model for investigating molecular mechanisms necessary  
17 for regenerating a functional nervous system. Numerous studies have led to the  
18 generation of extensive genomic resources, especially whole-animal single-cell RNA-  
19 seq resources. These have facilitated *in silico* predictions of neuronal subtypes, many of  
20 which have been anatomically mapped by *in situ* hybridization. However, our knowledge  
21 of the function of dozens of neuronal subtypes remains poorly understood. Previous  
22 investigations identified that *polycystic kidney disease (pkd)-like* genes in planarians are  
23 strongly expressed in sensory neurons and have roles in mechanosensation. Here, we  
24 examine the expression and function of all the *pkd* genes found in the *Schmidtea*  
25 *mediterranea* genome and map their expression in the asexual and hermaphroditic  
26 strains. Using custom behavioral assays, we test the function of *pkd* genes in response  
27 to mechanical stimulation and in food detection. Our work provides insight into the  
28 physiological function of sensory neuron populations and protocols for creating  
29 inexpensive automated setups for acquiring and analyzing mechanosensory stimulation  
30 in planarians.

31

## 32 Introduction

33 Freshwater planarians are an excellent organism to study stem cell-based regeneration  
34 due to their large population of stem cells and prodigious ability to regenerate all cell  
35 types, including neurons (Reddien, 2018; Ivankovic et al., 2019). The planarian nervous  
36 system is anatomically simple, but studies have demonstrated the neuronal population  
37 is highly heterogeneous, with many discrete cell types that are spatially restricted and  
38 give rise to form and function (Ross et al., 2017). From early estimates of dozens of  
39 specialized neuronal cell types, we do not know how many neuronal cell types or the  
40 exact functions of those cells in planarians (Fincher et al., 2018; Plass et al., 2018; King,  
41 H. O. et al., 2024). To fully comprehend how planarians regenerate neurons and restore  
42 function, generating a molecular neuroanatomical map and introducing tools to examine  
43 neuronal function will be critical. Efforts to create single-cell gene expression atlases  
44 have generated planarian cell-type profiles (Fincher et al., 2018; Plass et al., 2018;  
45 King, H. O. et al., 2024). Those studies have created two broad categories of neurons,  
46 ciliated and non-ciliated neurons, comprising the planarian nervous system (Fincher et  
47 al., 2018). Among the most prominent genes defining neural cells are *polycystic kidney*  
48 *disease-like* genes that define discrete ciliated neuronal populations, some of which  
49 have been implicated in mechanosensory and chemosensory functions (Fincher et al.,  
50 2018; Ross et al., 2018; Arnold et al., 2021).

51

52 PKD proteins are among one of the most ancient classes of sensory receptors. They  
53 are a member of the transient receptor potential (TRP) family of ion channels, which can  
54 be grouped into subfamilies based on the type of stimulus they are receptive to. The

55 infamous names of these genes come from their roles in autosomal dominant polycystic  
56 kidney disease (ADPKD) caused by mutations of the PKD1 or PKD2 genes that encode  
57 Polycystin-1 (PC1) and Polycystin-2 (PC2) proteins (Harris and Torres, 2009; Esarte  
58 Palomero et al., 2023). The rest of the PKD1 and -2 gene families consist of PKD1-LIKE  
59 and PKD2-LIKE proteins which are identified and grouped based on their structural and  
60 sequence similarities to the founding PC1 and -2 proteins (Esarte Palomero et al.,  
61 2023). PKD1 and PKD2 family members are integral membrane proteins that can exist  
62 as heterotetrameric receptor-like/ion channel complexes that transduce signals by  
63 conducting  $\text{Ca}^{2+}$  currents or potentially acting as a G-protein coupled receptor (Maser et  
64 al., 2022; Esarte Palomero et al., 2023). Multiple combinations of PKD1 family and  
65 PKD2 family members have been found in these heterotetramers creating a diverse  
66 array of complexes (Esarte Palomero et al 2023). This variety of complexes along with  
67 subcellular distribution - these proteins are found in multiple cellular locations, like the  
68 ER and primary cilia - implicate these proteins in diverse cellular processes in sensory  
69 neuron function, like mechanosensation and chemosensation, signal transduction and  
70 gene expression, gustatory sensing, and the sperm acrosome reaction (Esarte  
71 Palomero et al., 2023). Additionally, the evolutionary history and function of PKD genes  
72 is understudied. Homologs of PC1 proteins have not been found in invertebrate  
73 organisms and might represent vertebrate-specific gene duplication and evolution  
74 events. Thus, understanding the ancestral roles of PKD genes will benefit from studies  
75 in diverse organisms.

76

77 Most animals possess homologs of Pkd1- and Pkd2-like genes. Evidence from  
78 invertebrate model organisms, including acoels, planarians, *C. elegans*, *Hydra*, and  
79 *Nematostella vectensis*, indicate Pkd-like genes are expressed in nervous system cells  
80 (Barr et al., 2001; O'Hagan et al., 2014; McLaughlin, 2017; Fincher et al., 2018; Sebe-  
81 Pedros et al., 2018; Hulett et al., 2024; Sakagami et al., 2024). TRP channels have  
82 been noted to have an evolutionarily conserved role in mechanosensation and are  
83 present in a variety of organisms and clades (Liu and Montell, 2015). Across taxa, there  
84 is extensive variability in the roles of PKD channels. For example, Polycystin-2 can  
85 function without Polycystin-1 or be regulated by other receptors. In fission yeast, a Pkd2  
86 channel functions alone to sense the change in pressure during cytokinesis at the  
87 cleavage furrow and is required for proper cell division (Morris et al., 2019). In addition,  
88 *Drosophila* Pkd2 participates in phagocytosis of apoptotic cells (Van Goethem et al.,  
89 2012). In several sexually reproducing organisms, *pkd2* is expressed in sexual organs.  
90 In *C. elegans*, the Pkd-1 homolog *lov-1* and *pkd-2* are responsible for proper mating  
91 function in males (Barr et al., 2001; O'Hagan et al., 2014). In mice, there may be a role  
92 for *Pkd1L-3* and *Pkd2L-1* in the taste buds for sour taste detection (Ishimaru et al.,  
93 2006; Horio et al., 2011).

94

95 In planarians, Pkd genes are not expressed in the excretory organs (Thi-Kim Vu et al.,  
96 2015). Evidence from several studies indicates that Pkd1- and Pkd2-like genes, as well  
97 as other TRP genes, are expressed in sensory neurons (Inoue et al., 2014; Fincher et  
98 al., 2018; Ross et al., 2018; Arnold et al., 2021). Because of their striking expression  
99 patterns, abundant transcript levels, and essential roles in diverse cell physiology

100 processes, we sought to further characterize *pkd* homologs and examine unexplored  
101 family members. We performed comprehensive expression experiments in *S.*  
102 *mediterranea* *pkd* family genes and showed that they are expressed in neurons in  
103 asexual planarians. Moreover, expression analyses in sexually reproducing planarians  
104 revealed expression in the reproductive structures, suggesting *pkd* genes might also  
105 play roles in reproduction. We assessed *pkd* gene function using custom assays to  
106 characterize the physiological roles of *pkd*<sup>+</sup> sensory neurons in planarians. Furthermore,  
107 we describe simple setups for performing quantitative behavioral assays for  
108 mechanosensation and chemosensation. Our findings contribute to our understanding  
109 of planarian regeneration and neurobiology and will be useful for comparative studies of  
110 *pkd-like* gene evolution.

111

## 112 **Results**

### 113 **Planarian PKD Protein Domain Structure**

114 To determine if additional *pkd* genes were present in *S. mediterranea*, we extracted the  
115 highly conserved PKD domains from *pkd1L-2* and *pkd2L-1* as representatives of the  
116 *pkd1* and *pkd2* gene families, respectively, and ran BLAST searches against the  
117 planarian transcriptome (Rozanski et al., 2019). The searches revealed all nine known  
118 *pkd* transcripts, including six genes that we previously examined in (Ross et al., 2018)  
119 (Table S1), which is also consistent with the *pkd* homologs identified in (Thi-Kim Vu et  
120 al., 2015). We noted that two of these genes were categorized as alternative forms of  
121 the same transcript in the dd\_Smed\_v6 transcriptome (*pkd2L-2*: dd\_v6\_17348\_0\_3 and  
122 *pkd2L-3*: dd\_v6\_17348\_0\_2). However, these sequences do not align with each other  
123 and each sequence aligns with separate contigs in the *S. mediterranea* genome

124 (Grohme et al., 2018). These transcripts might represent two unique genes. Bayesian  
125 phylogenetic analyses support that the planarian *pkd* genes are clear homologs of  
126 PKD1-like (Fig. S1) and PKD2 and PKD2-like proteins (Fig. S2).

127  
128 We used PFAM to compare the domains in planarian PKD1 and PKD2 predicted  
129 proteins to the four PKD1 family proteins and three PKD2 (TRPP) family proteins found  
130 in humans. PKD2 family proteins are much smaller than PKD1 family proteins in general  
131 and *S. mediterranea* predicted proteins follow this trend similarly to the human proteins  
132 (Fig. 1A). Human PC1 is a larger protein than all other PKD-like proteins found in  
133 humans and planarians alike; PC1 is 4303 AA in length, more than 1.5X the size of the  
134 next largest human PKD family gene (PKD1L1), which is 2849 AA long (Fig 1A,  
135 Accession numbers in Methods). PC1 also contains several N-terminal extracellular  
136 domains located on the N-terminal side of the extracellular Receptor for Egg Jelly (REJ)  
137 domain that are not found in other PKD family proteins (Fig. 1A). Following these  
138 extracellular domains are eleven transmembrane domains with an intracellular  
139 polycystin-1, lipoxygenase, and  $\alpha$ -toxin (PLAT) domain that follows the first  
140 transmembrane domain. This domain was found in all human and planarian PKD  
141 sequences. A portion of the transmembrane sequence is classified as the highly  
142 conserved Polycystin Domain based on similarity to the PC1 sequence; this region is  
143 found in all PKD1 and -2 proteins in both humans and planarians. Finally, regions within  
144 both the PKD1 and -2 family proteins contain a highly conserved sequence known as  
145 the PKD cation channel (Fig. 1). Interestingly, although PKD1 proteins were historically  
146 known to function as receptors that cluster with one or more PKD2 genes that act as the

147 cation channel effector of this complex, recent research has shown that the last six  
148 transmembrane domains of PKD1 proteins are functioning as part of the cation  
149 channels (Esarte Palomero et al., 2023). There is evidence that PKD1 proteins form  
150 complexes with multiple PKD proteins (Esarte Palomero et al., 2023); given the  
151 conservation of domains seen between human and planarian PKD genes, it is possible  
152 that planarian PKD1 proteins form complexes with multiple PKD2 proteins as well.  
153

#### 154 **Planarian *pkd-like* genes are expressed in neurons**

155 To examine the expression of *pkd* genes in *S. mediterranea*, especially for the three  
156 untested genes, we performed whole-mount *in situ* hybridization (WISH) on intact  
157 asexual planarians. We observed labeling in multiple sensory-rich regions for all nine  
158 *pkd* genes (Fig. 1B). We also performed transverse cross-sections through the head  
159 regions of planarians to improve the spatial resolution of *pkd1L-1*, *pkd1L-3*, *pkd2-1*,  
160 *pkd2-4*, and *pkd2L-2*, which were expressed in the auricles and brain branches (Fig1B').  
161 Additionally, we performed WISH on chemically amputated pharynges to facilitate  
162 visualization of *pkd* labeling in pharyngeal tissues (Fig. 1C). Taken together, these  
163 experiments show that planarian *pkd* genes are strictly expressed in seven sensory cell-  
164 type rich structures and patterns (summarized in Table 1). Our results are consistent  
165 with *pkd* gene *in situ* experiments in other studies. Following on our previous work  
166 (Ross et al., 2018), we observed the expression of *pkd1L-2*, *pkd2-4*, *pkd2L-1*, and  
167 *pkd2L-2* in the rheosensory organ, which is comprised of the dorsal ciliated stripe as  
168 well as the ventral and dorsal peripheral stripes (highlighted with arrows, Fig. 1B and  
169 1B'). This population of cells represents submuscular neurons that are involved in

170 sensing mechanical stimulation, such as water flow and vibration (Ross et al., 2018).

171 *pkd1L-2* and *pkd2L-1* have the most discrete labeling patterns of all planarian *pkd*

172 genes; they are expressed in the rheosensory organ and in a small population of

173 photoreceptor neurons (Ross et al., 2018).

174

175 Five *pkd* genes, *pkd1L-1*, *pkd1L-3*, *pkd2-1*, *pkd2-4*, and *pkd2L-2*, were expressed in the

176 brain branches or auricles (Fig. 1B., yellow arrowheads). These structures have been

177 implicated in planarian chemosensation (Koehler, 1932; Fraenkel, 1961; Farnesi and

178 Tei, 1980; Roberts-Galbraith et al., 2016; Almazan et al., 2021). Most of these genes

179 were expressed in both anatomical regions (auricles, black arrowheads, and brain

180 branches, yellow arrowheads in Fig 1B') apart from *pkd1L-1* and *pkd1L-3*, which were

181 only expressed in the brain branches and auricles, respectively (Fig. 1B'). Additionally,

182 *pkd2L-2* expression extended well into the ventromedial brain (yellow arrows in Fig 1B

183 and 1B'). Interestingly, all *pkd* genes with expression in the auricle or the brain branches

184 were also expressed in populations of dispersed subepidermal cells. Expression of

185 *pkd1L-3* was previously attributed to both neurons and epidermal cells in Ross et al.

186 (2018) due to detectable transcript expression in a single *soxB1-2<sup>+</sup>* epidermal cell

187 identified in (Wurtzel et al., 2015). However, newer data does not strongly indicate

188 *pkd1L-3* expression in the epidermis (Fincher et al., 2018), which is consistent with our

189 observations. Four *pkd* genes, *pkd1L-1*, *pkd2-2*, *pkd2-3*, and *pkd2L-2*, were expressed

190 in the pharynx (red arrows, Fig. 1B and Fig. 1C). Expression patterns for *pkd2-2* and

191 *pkd2-3* looked nearly identical and were exclusively detected in the pharynx. In contrast,

192 *pkd1L-1* and *pkd2-4* had broader expression domains. All *pkd* genes expressed in the

193 pharynx had a similar pattern of expression throughout the pharynx with abundant  
194 expression at the distal end of the pharynx, in the pharyngeal nerve net. We did not  
195 observe *pkd* labeling in the protonephridia, consistent with reporting in Thi-Kim Vu et al.  
196 (2015).

197

198 We next sought to determine if the gene expression patterns correlated with cell-type  
199 assignments revealed by the single-cell RNA-seq atlas of whole-body planarian cells  
200 (Fincher et al., 2018). When we examined the enrichment of the *pkd* transcripts on  
201 scRNA-seq tSNE plots of *S. mediterranea* ciliated neurons, we observed a connection  
202 between *pkd*<sup>+</sup> WISH patterns and expression across the single cell clusters (Fig. 2).  
203 First, the genes expressed almost exclusively in the rheosensory organ (*pkd1L-2* and  
204 *pkd2L-1*) had clear enrichment in a small ciliated neural population (black circles, Fig.  
205 2B). Genes *pkd2-4* and *pkd2L-2*, which are also expressed in the rheosensory organ,  
206 also showed high levels of enrichment in this population (black circles in Fig. 2E). The  
207 transcript for *pkd2-2* was not present in the Fincher et al. dataset (Fincher et al., 2018),  
208 likely due to a discrepancy of this distinct transcript as an isoform of *pkd2-3*. We found  
209 that *pkd2-3* is spread in a series of subclusters (blue circle on the right side of the tSNE  
210 plot, Fig. 2D). The other *pkd* genes with expression in the pharynx (*pkd1L-1* and *pkd2L-*  
211 2) were similarly enriched throughout clusters in this subset of the plot (blue circles, Fig.  
212 2E). *pkd1L-3* and *pkd2-1*, which were expressed within populations of the brain  
213 branches, auricles, and dispersed subepidermal cells, displayed enrichment in a subset  
214 of clusters likely representing different neuronal cell types (red circle, Fig. 2C); *pkd1L-1*,  
215 *pkd2-4*, and *pkd2L-2* also showed expression in these regions by WISH and the

216 corresponding scRNA-seq populations amongst others (red circle, Fig. 2E). In our  
217 previous work, we showed that *pkd1L-2<sup>+</sup>* cells expressed pan-neural markers and the  
218 cilia gene, *rootletin* (Ross et al., 2018). Consistent with previous observations (Fincher  
219 et al., 2018), we detected co-enrichment of *rootletin* and pan-neuronal genes *synapsin*  
220 and *synaptotagmin* in the *pkd<sup>+</sup>* scRNA-seq clusters (Fig. 2F). We tested these  
221 observations by dFISH, which showed *pkd2L-2* is co-expressed with cilia and pan-  
222 neural markers (Fig. 2G).

223  
224 Because PKD proteins have been implicated in mating behaviors and reproduction in  
225 other organisms (Kierszenbaum, 2004; Esarte Palomero et al., 2023), we were intrigued  
226 if *pkd* genes could be detected near or in the reproductive structures of the *S.*  
227 *mediterranea* hermaphroditic strain (Issigonis and Newmark, 2019). Thus, we  
228 performed WISH to *pkd* genes in sexual planarians and found that in addition to the  
229 striking expression patterns observed in the asexual worms, *pkd1L-1*, *pkd1L-3*, *pkd2-1*,  
230 *pkd2-2*, *pkd2-4*, *pkd2L-1*, and *pkd2L-2* were expressed in the copulatory apparatus (Fig.  
231 S3). Furthermore, *pkd1L-2* was expressed in the copulatory apparatus, oviduct, and  
232 adjacent to the glands. *pkd2-3* was expressed in the copulatory apparatus and the  
233 testes; we also noted that *pkd2-1* and *pkd2-4* showed expression in the gonopore area.  
234 We do not know if the genes are expressed in reproductive cells or if neurons are  
235 adjacent to reproductive structures, but the robust expression suggests it will be  
236 interesting to investigate how *pkd* function impacts reproduction in *S. mediterranea*  
237 hermaphrodites. Taken together, the expression patterns of planarian *pkd* genes

238 demonstrate enrichment of expression in putative and previously characterized sensory  
239 neural populations.

240

#### 241 **Analysis of *pkd* gene expression regulation by SoxB1-2**

242 The *pkd*<sup>+</sup> sensory neuron clusters in the scRNA-seq plots suggest that these neuronal  
243 populations arise from divergent transcriptional regulatory networks. SoxB1-2 regulates  
244 six of the nine *pkd* genes (Ross et al., 2018); thus, in addition to previously  
245 characterized planarian *pkd* genes, we examined if *pkd1L-1*, *pkd2-2* and *pkd2-3* were  
246 impacted by *soxB1-2* activity. First, we analyzed *soxB1-2* expression in the single cell  
247 atlas and found that *soxB1-2* was expressed in the *pkd*<sup>+</sup> cluster group that represented  
248 brain branches and auricle expression as well as the cluster that represented  
249 rheosensory organ expression (red and black circles in Fig. 2A). *soxB1-2* expression  
250 was not detected in the group of clusters that corresponded with expression in the  
251 pharynx (Fig. 2D and 2E, blue circles). The six *pkd* genes that were previously identified  
252 as having reduced expression after *soxB1-2* RNAi had expression in both the red and  
253 black circled clusters. Thus, we investigated the impact of SoxB1-2 on *pkd* gene  
254 expression by performing RNAi for *soxB1-2* followed by WISH for *pkd* transcripts in both  
255 intact and regenerating fragments (RNAi scheme summarized in Fig 3A; results  
256 summarized in Table 1).

257

258 RNAi targeting *soxB1-2* resulted in a near to complete loss of *pkd* gene expression in  
259 the auricles (where *pkd1L-3*, *pkd2-1*, *pkd2-4*, and *pkd2L-2* are detected, black  
260 arrowheads in Fig. 3B), the rheosensory organ (arrows, Fig. 3B), and the dispersed

261 subepidermal cells (insets in Fig. 3B). Loss of *soxB1-2* function resulted in the loss of  
262 *pkd1L-3* and *pkd2-1* expression in nearly all areas of the brain branches but resulted in  
263 the loss of *pkd2-4* and *pkd2L-2* expression only in a subset of cells in the brain  
264 branches. There was no apparent loss of expression in the ventromedial brain region in  
265 *pkd2L-2*-labeled worms or in the photoreceptors in *pkd1L-2*-labeled worms. Finally,  
266 *soxB1-2* RNAi did not affect *pkd* gene expression in the pharynx (where *pkd1L-1*, *pkd2-*  
267 *2*, *pkd2-3*, and *pkd2L-2* were detected). These results in intact worms were consistent in  
268 regenerating worms, except for *pkd1L-2* and *pkd2L-1* detection in a few anterior and  
269 posterior regenerated cells (Fig. 3C-D). Therefore, two of the *pkd* genes that were not  
270 previously identified as downstream of *soxB1-2* activity were, indeed, unaffected by  
271 *soxB1-2* RNAi; expression of *pkd2-2* and *pkd2-3* in the pharynx were comparable  
272 between controls and *soxB1-2(RNAi)* worms. This is consistent with the lack of  
273 overlapping expression gleaned from the scRNA-seq dataset (Fig. 2). Interestingly,  
274 *pkd1L-1* expression was downregulated following *soxB1-2* RNAi, but only in the brain  
275 branches and dispersed subepidermal cells and not the pharynx, which might explain  
276 why it was not detected as a differentially expressed gene in our published *soxB1-2*  
277 RNA-seq dataset (Ross et al., 2018).

278

### 279 **A subset of PKD genes is required for mechanosensation**

280 Past studies, including classic literature, indicated that the dorsal ciliated stripe functions  
281 as a water-sensing organ (rheosensing), i.e., as a mechanosensing organ. At present, it  
282 is impractical to assess the neurophysiological properties of most neurons in planarians;  
283 therefore, we designed behavioral tests that could be used as readouts of impaired

284 neurophysiological activity. Thus, we previously showed that disrupting *pkd1L-2* and  
285 *pkd2L-1* function using RNAi impairs rheosensation and vibration sensation (Ross et al.,  
286 2018). In addition, we described abnormal locomotion resulting from *pkd2-4* RNAi,  
287 including slow, inching, jerky movements that precluded inclusion in further behavioral  
288 assays. As a result, we sought to modify our RNAi scheme so that the onset of the  
289 *pkd2-4* RNAi phenotype requires longer to manifest, allowing us to perform behavioral  
290 analysis. Using this scheme (see Fig. S4A), we recorded animal movement defects by  
291 day 55 of the RNAi protocol; normal movements were recorded throughout behavioral  
292 assays (see reduced and extended feeding schemes and testing times in Fig. S4A-B  
293 and VideosS1-4 of normal movement for behavioral assays and extended feeding  
294 movement defects).

295

296 To determine if any additional *pkd* genes are required for mechanosensation, we  
297 employed the Ross et al. (Ross et al., 2018) vibration assay with modifications (see  
298 Methods and Fig. S4C-D). Control worms reliably contracted their bodies along the  
299 anteroposterior axis following a tapping stimulus; we measured responses by  
300 calculating the percent change in body length between pre-stimulus gliding length and  
301 post-stimulus length. We found that *pkd1L-2*, *pkd2L-1*, and *pkd2-4* RNAi displayed a  
302 significant decrease in response to the stimulus, while all other *pkd* genes had a similar  
303 contraction response as the controls (Fig. 4). We previously found that worms with a  
304 reduced ability to sense vibration in the water had a decreased ability to sense water  
305 flow applied across their dorsal side and, as with the vibration assay, lacked a normal  
306 contraction response (Ross et al., 2018). Therefore, we performed a rheosensory assay

307 for the *pkd* genes showing a vibration defect (Fig. S4E). As an additional control, we  
308 also analyzed *pkd1L-3*, which is not expressed in the rheosensory organ. We found that  
309 the same three genes recapitulated a mechanosensory defect phenotype: *pkd1L-2*,  
310 *pkd2L-1*, and *pkd2-4* (Fig. S4F-G). Each of these transcripts was expressed in the  
311 dorsal ciliated stripe, implicating them as essential for the mechanosensory function of  
312 these neurons.

313

314 **PKD genes required for chemosensation**

315 Studies in vertebrate and invertebrate models implicate *pkd* gene function in  
316 chemosensory functions (LopezJimenez et al., 2006; Horio et al., 2011; O'Hagan et al.,  
317 2014). We observed the expression of five planarian *pkd* genes in the auricles and brain  
318 branches and the expression of four *pkd* genes in the pharynx (structures linked to  
319 chemosensory functions) (reviewed in Ross et al., 2017; Miyamoto et al., 2020). Thus,  
320 we investigated if planarian *pkd* gene function may be required for chemosensation. In  
321 our previous work, we noted reductions in the time *pkd2-1* and *pkd2L-1* RNAi worms  
322 spent in a 'food zone' of a circular dish, but without statistical confidence (Ross et al.,  
323 2018). To improve our analysis of chemosensory behaviors, we modified our assay  
324 (Fig. S5 and Methods). Using the modified assay, we found that of the intact worm  
325 groups, only *pkd2-4(RNAi)* worms showed a significant decrease in the time spent in  
326 the food zone. No groups showed a significant difference in the percent of worms that  
327 ate during the assay (Fig. 5A). However, in regenerates, both *pkd1L-1(RNAi)* and *pkd2-*  
328 *4(RNAi)* worms showed significant decreases in both the time in food zone and the  
329 percent of worms that ate during the assay (Fig. 5B). Both genes were expressed in the

330 brain branches and *pkd2-4* was also expressed in the auricle area, indicating that cells  
331 within these structures are involved in chemosensing. While *pkd1L-1* is additionally  
332 expressed in the pharynx, other pharynx-expressed *pkd* genes had no significant  
333 feeding defects; we do not know at this time what role these *pkd* genes might be playing  
334 in mechanosensation or chemosensation in the pharynx. However, the overall reduced  
335 time in the food zone seen with loss of function of *pkd1L-1* and *pkd2-4* suggests the  
336 RNAi-treated planarians are unable to detect food in the water and hence fail to track  
337 the pellets in the first place, which attributes this phenotype to chemosensation. There  
338 are known roles for *pkd* genes in taste in other organisms (LopezJimenez et al., 2006;  
339 Horio et al., 2011), which might explain the abundant presence of some *pkd* genes in  
340 the tip of the pharynx; however, our experiments did not uncover defects that could be  
341 attributed to pharyngeal gene expression.

342

### 343 **Co-expression of PKD1 and PKD2 family members in sensory neurons**

344 PKD1 and PKD2 proteins are known to work cooperatively in cilia to facilitate sensory  
345 signal input, with PKD1 proteins acting as a receptor and PKD2 proteins acting as an  
346 ion channel (Esarte Palomero et al., 2023). We observed reduced chemosensing  
347 behavior with loss of *pkd1L-1* and *pkd2-4* expression (Fig. 5) and reduced  
348 mechanosensation when *pkd1L-2*, *pkd2L-1*, and *pkd2-4* were inhibited individually (Fig.  
349 4). Because of the overlapping expression of *pkd1L-1* and *pkd2-4* in multiple scRNA-  
350 seq clusters (red circle, Fig. 2E) and expression of all three *pkd* genes that resulted in  
351 mechanosensory defects in the rheosensory organ scRNA-seq cluster (black circle, Fig.  
352 2B and 2E), we reasoned that genes expressed in the same scRNA-seq clusters with

353 behavioral phenotypes likely function in the same cells. Due to the known relationship  
354 between PKD1 and PKD2 proteins, we sought to determine if the pairs of *pkd1-like* and  
355 *pkd2* genes resulting in behavioral phenotypes were co-expressed using double-  
356 fluorescent in situ hybridizations (dFISH).

357

358 First, we performed dFISH on *pkd1L-1* and *pkd2-4* and observed co-expression in cells  
359 throughout the brain branch region in both ventromedial and dorsolateral cells (arrows  
360 and inset image in Fig 6A ventral and dorsal). *pkd2-4* labeling was much more  
361 abundant, which is in line with the increased number of cells that appear to have  
362 expression in both the WISH labeling (Fig. 1) and scRNA-seq tSNE plots (Fig. 2). Thus,  
363 it was not surprising that we were also able to see multiple cells in the head region that  
364 were only labeled with *pkd2-4* and not *pkd1L-1* (arrowheads in Fig. 6). Next, we  
365 examined co-labeling of the *pkd1* and -2 genes that resulted in mechanosensory  
366 phenotypes. *pkd1L-2* had very discrete labeling patterns by WISH and in the scRNA-  
367 seq plots, almost exclusively in the rheosensory organ (except for faint photoreceptor  
368 staining). However, we know of at least two distinct populations of cells in the  
369 rheosensory organ (one marked by *pkd1L-2* and the other by *hemicentin-1-like*) (Ross  
370 et al., 2018). So, we were uncertain whether these *pkd*<sup>+</sup> cells represented the same or  
371 distinct populations. We performed dFISH with these genes and found that these genes  
372 were, indeed, labeling the same discrete population of cells (white arrows and inset, Fig.  
373 6). We also examined if *pkd2-4* was expressed in this cell population and found that  
374 *pkd1L-2* cells expressed *pkd2-4* (Fig. 6B, arrows); we again observed many additional

375 cells labeled solely by *pkd2-4* (Fig. 6B, arrowheads). Thus, our data suggest that PKD1  
376 and PKD2 genes function together in subsets of sensory cells.

377

## 378 **Discussion**

### 379 ***pkd* genes are expressed in neurons distributed across the body and pharynx of** 380 **planarians**

381 Previous work revealed that *pkd* genes are expressed in sensory regions and play roles  
382 in processes like sensing water flow or vibration in planarians. Here, we sought to  
383 characterize all *pkd* family members, including the *S. mediterranea* homologs, *pkd1L-1*,  
384 *pkd2-2*, and *pkd2-3*, that had yet to be analyzed. The planarian nervous system is  
385 surprisingly heterogeneous, with many specialized cell types that can be predominantly  
386 distinguished by unique gene expression signatures. Combined with previous reports,  
387 we conclude that *pkd* genes are exclusively expressed in neuronal cells in the asexual  
388 *S. mediterranea* biotype. This observation is consistent with previous reports indicating  
389 *pkd* genes are not expressed in the planarian ciliated excretory cell types, and we did  
390 not observe the types of phenotypes associated with protonephridia defects, such as  
391 osmoregulatory defects like bloating.

392

393 Because of the known roles of *pkd* genes in mating behaviors and reproductive  
394 processes in divergent organisms like *C. elegans*, *Drosophila*, sea urchins, and  
395 humans, curiosity drove us to examine the expression of *pkd* genes in the  
396 hermaphroditic strain of *S. mediterranea* (Fig. S3). The analysis yielded more questions  
397 than answers, opening the door to a future study to assess *pkd* genes' specific cell-type

398 expression and roles in mating behavior or fertilization. In addition to the neuronal  
399 patterns observed in asexual worms, we observed striking expression in reproductive  
400 organ anatomical regions of mature *S. mediterranea* hermaphrodites. However, we do  
401 not know the identities of the cells expressing *pkd* genes in the reproductive organs,  
402 which will require future experimentation to resolve if genes are expressed in sensory  
403 neurons or in reproductive somatic and gonadal cells. A recent study generated scRNA-  
404 seq data for the sexual biotype (Issigonis et al., 2024), so this new resource could  
405 advance the identification of cell types before performing double *in situ* hybridization  
406 experiments in hermaphrodites to provide insight into the cell-type expression of *pkd*  
407 genes. Interestingly, Pkd2 is found in sperm, and its function is required for fertilization  
408 (Gao et al., 2003; Watnick et al., 2003; Kierszenbaum, 2004). We observed *pkd2-3*  
409 expression in the planarian testes, suggesting it will be interesting to investigate  
410 whether it plays a conserved role in male fertility.

411

#### 412 ***pkd* gene roles in sensory reception and behavior**

413 We extended previous findings using behavioral assays showing that *pkd* genes have  
414 robust roles in mechanosensory and chemosensory reception (Ross et al., 2018). Our  
415 data supports that *pkd1L-2*, *pkd2-4*, and *pkd2L-1* are required for the mechanosensory  
416 function of the sensory population along the dorsal and peripheral ciliated stripes.  
417 Interestingly, gene co-expression analysis showed that these transcripts are expressed  
418 in the same neurons. Based on the canonical function of Polycystin-1 proteins, we  
419 surmise that *pkd1L-2* regulates the activity of *pkd2-4* and *pkd2L-1* (Fedele et al.,  
420 2014). We hypothesize that *pkd1L-2* acts as the receptor and couples the mechanical

421 stimulation to either *pkd2-4* or *pkd2L-1* channels. Although double-FISH revealed the  
422 expression of both transcripts in double-positive cells, concluding that these proteins are  
423 co-localized or working together would require other approaches, like generating  
424 antibodies for protein immunostaining or biochemical assays.

425

426 Furthermore, we found that *pkd1L-1* and *pkd2-4* have roles in the chemosensory  
427 behaviors associated with feeding (Fig. 5). These genes were expressed in the brain  
428 branches and *pkd2-4* was also expressed in the auricle area, strongly indicating that  
429 cells within these structures are involved in chemosensation. Conversely, we did not  
430 observe phenotypes for *pkd2-2* and *pkd2-3*, which were specifically expressed in the  
431 pharynx. However, we did not directly test nor quantify pharyngeal behavior as in  
432 Miyamoto et al. (2020). Thus, it remains possible that pharyngeal *pkd* genes have roles  
433 in chemosensation. From our phenotype analysis, we can conclude that *pkd1L-1* and  
434 *pkd2-4* implicate head neurons in chemotaxis behaviors independent of the pharynx.  
435 *pkd1L-1* RNAi phenotypes were only observed in regenerates, suggesting stronger  
436 penetrance when the animals were challenged to fully regenerate heads.

437

438 We sought to redesign rigorous assays for straightforward set up and implementation  
439 (see Methods) that are based on our previous work (Ross et al., 2018); unfortunately,  
440 the code for the published assays was no longer available (the data was lost in a  
441 computer hardware failure; E.-M. S. Collins, personal communication). Our redesigned  
442 assays complement other existing assays to measure locomotion and other modalities  
443 like thermotaxis and thigmotaxis (Inoue and Agata, 2022). Because we only challenged

444 the RNAi groups with assays related to mechanosensory and chemosensory abilities  
445 due to the defects seen in *soxB1-2* and downstream genes, other assays, such as  
446 thermosensation and thigmotaxis could reveal roles for some of the genes in this  
447 screen, especially the PKD2 family genes, which fall within the TRP family and have  
448 been demonstrated to function independently of PKD1 family members (Esarte  
449 Palomero et al., 2023). It has already been shown in *D. japonica* that *trpm3* participates  
450 in thermosensation (Inoue et al., 2014). It is possible *pkd* genes are involved in other  
451 sensory modalities like detection of chemical changes or temperature that have been  
452 shown to influence behaviors like reactions to water currents in other planarian species  
453 (Allen, 1915). In addition, further exploration using the scRNA-seq datasets for *S.*  
454 *mediterranea* could uncover other gene signatures that could help predict functions of  
455 the *pkd<sup>+</sup>* cell populations in the auricles or the pharynx.

456

#### 457 **Concluding Remarks**

458 This study sought to characterize the role of *pkd* genes in sensory neuron regeneration  
459 and function in the planarian *S. mediterranea*. In vertebrates, PKD1 and PKD2 genes  
460 are expressed in excretory organs and mutations in either protein causes Autosomal  
461 Dominant Polycystic Kidney Disease; however, studies have increasingly implicated  
462 PKD family genes in neural development and functions like taste reception (Harris and  
463 Torres, 2009; Ohata et al., 2015; England et al., 2017). In many invertebrates, including  
464 planarians, Pkd-like genes are expressed in nervous system cells (Barr et al., 2001;  
465 O'Hagan et al., 2014; McLaughlin, 2017; Fincher et al., 2018; Ross et al., 2018; Sebe-  
466 Pedros et al., 2018; Hulett et al., 2023; Sakagami et al., 2024). Consistent with those

467 observations, *pkd* genes have strong expression in ciliated sensory neurons and have  
468 functions in sensory reception in *S. mediterranea*. Although additional evidence is  
469 required, it is tempting to speculate that an ancestral function of Pkd-like proteins is in  
470 sensory reception and is later co-opted in other organs like the vertebrate kidney. This  
471 work contributes to knowledge of *pkd* gene function in the Platyhelminthes, which will be  
472 useful for comparative studies on the evolution of neuronal functions.

473

#### 474 **Acknowledgements**

475 This study was supported by a California Institute for Regenerative Medicine Grant  
476 EDUC4-12813 postdoctoral fellowship to M.A. and NIH R01GM135657 to RMZ. We  
477 thank Dr. Yusuf Ozturk for help with the Arduino code; Lia Escobar and Malia Huff for  
478 help collecting PKD homolog sequences for phylogenetic analysis. Portions of the  
479 assay design cartoons were created with BioRender.com.

480

481 **Methods**

482 **Planarian care**

483 Asexual planarians (CIW4) were maintained in 1X Montjuïc salts (1.6 mM NaCl, 1.0 mM  
484 CaCl<sub>2</sub>, 1.0 mM MgSO<sub>4</sub>, 0.1 mM MgCl<sub>2</sub>, 0.1 mM KCl, 1.2 mM NaHCO<sub>3</sub>) in plastic  
485 containers in an incubator at 20°C. Worms were fed homogenized liver and cleaned  
486 once per week. Planarians were starved one week prior to RNAi and fixation for in situ  
487 experiments.

488

489 **Cloning PKD genes**

490 Nine PKD genes were previously identified by Thi-Kim Vu et al. (2015). We used the  
491 Conserved Domain Database to extract the PKD\_Channel domain from *pkd1L-1*  
492 (dd\_Smed\_v6\_13975\_0\_1) and *pkd2L-1* (dd\_Smed\_v6\_15626\_0\_1) (Wang et al.,  
493 2023) and then translated the domain sequences on Expasy  
494 (<https://web.expasy.org/translate/>). We entered these peptide sequences into the  
495 BLAST tool at PlanMine (Rozanski et al., 2019) and performed a TBLASTN search  
496 against the dd\_Smed\_v6 transcriptome with an expected e-value cut-off of e<sup>-10</sup>, which  
497 returned the nine PKD genes that were previously identified. The results were saved as  
498 Table S1. Genes fragments were cloned from cDNA or were purchased as pre-  
499 synthesized nucleotide eBlocks from Integrated DNA Technologies,  
500 <https://www.idtdna.com/> (Table S2). Fragments were inserted into pPR242-T4P using  
501 ligation-independent cloning and transformed into HT115 (Adler and Alvarado, 2018).  
502 Primers, cDNA sequences, and eBlock fragment sequences for genes used in this  
503 paper are listed in Table S2.

504

505 **PKD protein domain comparison to human Polycystin proteins**

506 *S. mediterranea* *pkd* transcript sequences and human PC-1 (P98161), PKD1L-1  
507 (Q8TDX9), PKD1L-2 (Q7Z442), PKD1L-3 (Q7Z443), PC-2 (Q13563), PKD2L-1  
508 (Q9P0L9), PKD2L-2 (Q9NZM6) protein sequences were uploaded into the legacy Pfam  
509 website, version 35 (pfam-legacy.xfam.org) using the search function with an expected-  
510 value cutoff set to 1.0. In all instances where transcripts were used, only one frame  
511 demonstrated significant hits to domains. The domain information was copied from  
512 Pfam, and representative images were created copying all domains represented in  
513 Pfam.

514

515 **Phylogenetic analysis**

516 The software Geneious ([www.geneious.com](http://www.geneious.com)) was used to create a multiple alignment  
517 using the MUSCLE 5.1 plugin (Edgar, 2022). Protein alignments were manually  
518 inspected, and the PKD Channel Domains (aligned to the human Pfam PKD1 and  
519 PKD2 cation channel domains listed in Supplementary Files 1-2) were extracted for  
520 performing Bayesian inference of phylogeny using the MrBayes 3.2.6 (Huelsenbeck and  
521 Ronquist, 2001) plugin developed by Marc Suchard and the Geneious Team with the  
522 following settings: unconstrained branch length, shape parameter exponential of 10,  
523 1.1Million chain length, 4 heated chains, 0.2 heated chain temp., WAG substitution  
524 model, gamma rate variation model, 10% burnin length with subsampling frequency of  
525 200. All sequences used and the protein alignments are provided in Supplementary  
526 Files S1-4.

527

528 **Whole-mount in situ hybridization**

529 Riboprobes were synthesized using either digoxigenin-11-UTP (DIG, Roche) or  
530 dinitrophenol-11-UTP (DNP, Perkin Elmer) as described in King, R. S. and Newmark  
531 (2013). Whole-mount in-situ hybridizations were performed on asexual planarians as  
532 previously described (King, R. S. and Newmark, 2013)<sup>[39]</sup>, except for the addition of a  
533 1.5 or 3 minute incubation in a reduction solution (50 mM DTT, 1% NP-40, 0.5% SDS in  
534 1X PBS) after fixation as in (Pearson et al., 2009). Hybridization and post-hybridization  
535 wash steps were performed at either 56°C or 58°C. Chromogenic asexual WISH  
536 samples were incubated with anti-DIG-AP (1:2000) and then developed with an NBT-  
537 BCIP solution (Roche) as previously described (King, R. S. and Newmark, 2013).

538 Fixation and processing of sexual *S. mediterranea* for whole-mount in-situ  
539 hybridizations were performed as described in Issigonis et al. (2022) on worms  
540 approximately 8 mm in length that were checked visually for the presence of the  
541 gonopore prior to experimentation. The following exceptions were made to the protocol:  
542 animals were incubated in reduction solution (50 mM DTT, 1%NP-40, 0.5% SDS, in  
543 PBS) for 5 min at 37°C after being fixed. The hybridization protocol was performed as  
544 described in (King, R. S. and Newmark, 2013) except the hybridization time was  
545 increased to 36 hours, and four extra 0.1X SSCx (SSC + 0.1% Triton X-100) washes  
546 were performed post-hybridization. For WISH on isolated pharynxes, we followed a  
547 chemical amputation for pharynx removal as described in Miyamoto et al. (2020) and  
548 performed the fixation and WISH protocol as in King, R. S. and Newmark (2013). dFISH  
549 samples were fixed and hybridized in a mixture of the DIG and DNP probes, as

described above. After SSCx washes, samples were washed twice in TNTx (0.1 M Tris pH 7.5, 0.15 M NaCl, 0.3% Triton X-100) at room temperature for 10 minutes, blocked in TNTx-blocking solution (5% heat-inactivated horse serum, 5% Roche Western Blocking Buffer in TNTx) and then incubated in anti-DNP-POD (Vector Laboratories, 1:2000) in TNTx-blocking solution overnight at 4°C. Samples were then washed six times for 20 minutes at room temperature in TNTx and then developed with Cy3-Tyramide as described in (King et al 2013). After MABTw (Maleic Acid Buffer + 0.1% Tween-20) washes, animals were incubated in MABTw blocking solution (5% heat-inactivated horse serum, 5% Roche Western Blocking Buffer in MABTw) for 2 hours at room temperature and then incubated in anti-DIG-AP (Roche, 1:2000) overnight at 4°C and washed and developed with Fast Blue as described in (King 2013). After post-development washes, samples were quenched with CuSO<sub>4</sub> solution (10mM CuSO<sub>4</sub>, 50mM ammonium acetate pH5.0) for 1 hour at room temperature, washed in ultrapure water two times for 5 minutes at room temperature and then with PBSTx 2 times for 5 minutes at room temperature, and incubated overnight in 5 ug/ml DAPI in PBSTx at 4°C. Worms were mounted in 80% glycerol or a 1:1 mixture of 80% glycerol and Vectashield under a No. 1 thickness cover glass and imaged on a Leica M250C stereomicroscope fitted with a Leica DFC 450 color camera for chromogenic WISH or Leica Stellaris 5 Confocal microscope running LAS X v4.6.1 with a 20x/0.75 dry objective. dFISH images were acquired through the Z-plane of the region of interest at the optimal interval identified by the software and further processed to extract slices of interest, create a maximum intensity projection, and overlay multiple pseudocolored channels in either FIJI (ImageJ2 version 2.9.0) (Schindelin et al., 2012) or LAS X.

573

574 **RNA interference**

575 Double-stranded RNA was synthesized by bacterial expression (Adler and Alvarado,  
576 2018) or *in vitro* transcription reactions using the MEGAscript T7 RNA synthesis kit  
577 (Invitrogen, Inc) as described in (Rouhana et al., 2013). For *in vitro* dsRNA, the  
578 synthesized dsRNA was diluted to a concentration of 1 µg/µl and stored in DEPC-  
579 treated water at -20°C. The pellets were freshly prepared by mixing the liver extracts  
580 with an agarose solution (1.25 µl of Liver extract + 0.25 µl of 2% low-melting agarose  
581 and 0.5 µl of dsRNA per planarian in the dish) and then frozen for approximately one  
582 hour before feeding. For the non-extended feeding protocol, planarians were fed either  
583 bacterially expressed or *in vitro* transcribed dsRNA liver pellets eight times over 4  
584 weeks. Extended-feed RNAi planarians were fed 14 times over 7 weeks.

585

586 **Vibration assay**

587 Vibration assays were performed the day following completion of RNAi feeding as well  
588 as on planarians that regenerated their heads 13-15 days following amputation anterior  
589 to the pharynx. Groups of 5 planarians were placed near the center of a 100 mm  
590 diameter petri dish filled with 40 mL of Montjuïc salts that was anchored with silicone  
591 paste into a plate lid fixed onto a cold LED board. The setup is illustrated in (Fig. S4C-  
592 C'). After worms were gliding normally, a tapping program (code in Supplementary File  
593 S5) running from a microcontroller board (Arduino Uno Rev3) connected to a Seamuing  
594 MG996R Micro Servo motor (Model No. 5123164-2360-1341090661) with an attached  
595 plastic arm that was 112 mm in length from the center of the rotor to the end of the arm,

596 4 mm thick, and 8 mm wide (obtained from Fielect 75 Type Plastic Gears Kit  
597 FLT20191223S-1008 from amazon.com). The end of the arm, wherein the tapper struck  
598 the dish, was wrapped with laboratory tape to increase the thickness to approximately 8  
599 mm in thickness. Taping also served to dampen the vibration of the arm during the  
600 tapping stimulus. The mechanism was programmed to deliver five taps at a rate of one  
601 tap every 75 ms to the side of the dish. Supplementary File S5 provides a link to the  
602 code used to control a Servo motor from an Arduino board (Supplementary File S5).

603

604 **Rheosensation assay**

605 Rheosensory assays (Fig. S4E) were performed the day following completion of RNAi  
606 feeding and on planarians that regenerated their heads 13-15 days following amputation  
607 anterior to the pharynx. A single asexual worm was placed inside a clear plastic  
608 chamber with dimensions of 90 mm in length by 40 mm in height filled with 10 ml of 1X  
609 Montjuïc salts and observed until gliding normally and parallel to the front of the  
610 chamber, in some cases, the planarian would need to be pipetted with a transfer pipet  
611 and moved to help orient them back into the middle of the chamber. Then, 30 µl of  
612 ultrapure water containing yellow food dye was ejected on the dorsal side of the worm  
613 using a Finnpipette P50 (50 µl) pipette.

614

615 **Chemosensation assay**

616 Food pellets were prepared by making a gelled liver paste containing a ratio of 25 µl of  
617 liver paste (500 µl of pureed liver mixed with 460 µl of ultrapure water and 40 µl red food  
618 coloring) to 5 µl of 2% low melting point agarose and then pipetting 15 µl drops of gelled

619 liver paste onto wax paper which were then frozen at -20°C for at least 1 hr.  
620 Chemosensory assays were performed in a clear plastic STORi 6" x 3" X 2" stackable  
621 bin (purchased from amazon.com). The dimensions of the bottom of the rectangular tray  
622 were 140 mm x 65 mm and contained marks for a 'start zone' line 10 mm away from the  
623 end of the tray and a food line 80 mm away from the 'start zone' line with lines 5 mm  
624 from either side of the food line to denote the 'food zone' (see Figure S5 for tray  
625 illustration). The tray was filled with 50 ml of 1X Montjuïc salts, and then three of the  
626 gelled liver paste pellets were placed across the food zone line. The food was allowed  
627 three minutes of diffusion time in the water, and then 10 worms from either the control  
628 or experimental group were transferred into the 'start zone' and allowed a 10-minute  
629 time frame to glide 2/3 distance across a 140 mm dish to a 10 mm 'food zone' where 3  
630 agarose-liver pellets were placed, and where chemical signals emanating from the food  
631 pellets would be strongest (Fig. S5A). We analyzed videos of the worms during the 10-  
632 minute assay and measured both the total time that planarians spent within the 'food  
633 zone' as well as the total number of worms that consumed food during that period for  
634 both intact and regenerate worms (RNAi scheme summarized in Fig. S4B). Worms  
635 were visually inspected for red food dye, and the number of worms that ate were  
636 recorded in addition to the analysis described below.

637

### 638 **Behavioral assay digital recording and video analysis**

639 All behavioral assays were recorded using a Basler Ace 2 Pro ac1440-220uc camera  
640 recording onto a PC running Basler's pylon Viewer 64-bit version 6.3.0 software at a  
641 frame rate of 10 frames/second and frame size of 1440 x 1080 pixels. *gfp(RNAi)*

642 planarians were used as the control group for all experiments. Video frames were  
643 analyzed in FIJI (ImageJ2 version 2.9.0) (Schindelin et al., 2012). For Vibration and  
644 Rheosensory assays, the line tool in FIJI was used to measure the longest pre-stimulus  
645 length of each gliding worm and the length of the worm following application of the  
646 stimulus. The percent change in the length was calculated as Percent Change =  
647  $[(\text{Length}_{\text{Pre-Stimulus}} - \text{Length}_{\text{Post-Stimulus}}) / \text{Length}_{\text{Pre-Stimulus}}] \times 100$ . For the chemosensory  
648 assay, the worms were tracked visually one at a time within frames to determine every  
649 timepoint when that worm entered and exited the food zone. The sum of all time (in  
650 seconds) spent in the food zone during the 10-minute assay period was calculated. For  
651 all behavioral experiments, measurements were collected for at least 10 worms per  
652 experimental group over at least two independent experiments.

653

#### 654 **Statistical analysis**

655 All statistical analyses were performed in GraphPad Prism 9, and graphs were created  
656 in the same software. One-way ANOVA was performed and corrected for multiple  
657 comparisons using Dunnett's correction. All means were compared to a *gfp* control  
658 group. Statistical significance was accepted at values of  $p < 0.01$ .

659

660 **Figure Legends**

661 **Figure 1. Predicted domain structures of human and planarians and whole-mount**  
662 **in situ hybridizations in asexual *Schmidtea mediterranea*.** The protein domains of  
663 PKD1 and PKD2, human and planarian proteins, illustrate the conserved presence of  
664 key structural and functional domains in these proteins. REJ, Receptor for Egg Jelly;  
665 GPCR, G-Protein Coupled Receptor; PLAT, Polycystin-1, Lipoxygenase, and alpha  
666 toxin; WSC, cell wall integrity and stress response component. The exception is the  
667 PKD1 (Polycystin-1) protein, which has been only found in chordates and possesses a  
668 complex N-terminal extracellular domain. (B) *pkd* gene WISH in asexual planarians  
669 reveals a variety of expression patterns, including expression in dispersed subepidermal  
670 cells, in the dorsal ciliated stripe and peripheral stripes (black arrows), in the pharynx  
671 (red arrows), photoreceptors (white arrows), in the auricles and brain branches (yellow  
672 arrowheads), and in the brain (yellow arrows). Scale bars, 200 µm. (B') Cross-sections  
673 of WISH from (B) of brain branch- and auricle-expressed *pkd* genes highlight  
674 expression in either the brain branches (black arrowheads), the auricle region (yellow  
675 arrowheads), and the brain (yellow arrows). Expression in the dorsal ciliated stripe is  
676 highlighted with black arrows. Scale bars, 100 µm. (C) WISH on isolated pharynges for  
677 genes with pharyngeal expression shows the expression of *pkd* transcripts in discrete  
678 puncta throughout the pharynx and abundant expression in the pharyngeal nerve net at  
679 the distal end (bottom of each image). Scale bars, 50 µm. n ≥ 8 worms tested, with all  
680 worms displaying similar expression patterns for all genes.

681

682 **Figure 2. Planarian scRNA-seq tSNE plots demonstrate that *pkd<sup>+</sup>* cells are ciliated**  
683 **neuronal cells and that a subpopulation of *pkd<sup>+</sup>* cells co-express *soxB1-2*. (A-F)**  
684 tSNE plots for all *pkd* genes were downloaded from <https://digiworm.wi.mit.edu/>  
685 (Fincher et al., 2018). Each dot represents a single cell, with the relative expression of  
686 the gene represented as the color of the dot, as defined by the heatmap on the right  
687 side of each tSNE plot. (A) *soxB1-2* is expressed in clusters that contain the *pkd<sup>+</sup>*  
688 mechanosensory (rheosensory) population (black circle) and the *pkd<sup>+</sup>* chemosensory  
689 populations (clusters within the red outline). (B-F) tSNE plots for all the *pkd* genes  
690 except for *pkd2-2*, which is not represented in the Fincher et al. (2018) dataset. Broadly,  
691 *pkd* genes are expressed in one or more of three groupings of clusters which  
692 correspond to expression patterns seen in the whole animal (see Figure 2): the  
693 rheosensory organ cluster (black circle), the brain branch and auricle cluster (red  
694 outline), and the pharynx cluster (blue outline). (B) *pkd1L-2* and *pkd2L-1* are expressed  
695 in the rheosensory organ cluster (black circle). (C) *pkd1L-3* and *pkd2-1* expression is  
696 visualized in the brain branch and auricle clusters (red outline). (D) *pkd2-3* is expressed  
697 in the pharynx clusters (blue outline). (E) *pkd1L-1*, *pkd2-4*, and *pkd2L-2* are expressed  
698 in multiple clusters, as highlighted by outlining the pertinent clusters on the tSNE plots.  
699 (F) Co-expression of pan-neural (*synapsin* and *synaptotagmin*) and cilia (*rootletin*)  
700 marker genes in the *pkd<sup>+</sup>* clusters indicate that these cells are ciliated neurons. (G) to  
701 further confirm that co-expression of *synapsin*, *synaptotagmin*, and *rootletin* in *pkd<sup>+</sup>*  
702 clusters in the single cell data correlates with gene expression in the animal, the co-  
703 expression of these markers (green; *ciliated* = *rootletin*, *neural* =  
704 *synapsin/synaptotagmin mix*) with *pkd2L-2* (magenta) is shown. Dashed boxes

705 represent the area of the inset in the images. Scale bars, 50 µm, n ≥ 3 worms tested  
706 with all samples displaying similar expression patterns.  
707

708 **Figure 3. SoxB1-2 positively regulates *pkd* gene expression in sensory**  
709 **populations.** (A) Timeline for assaying *pkd* gene expression by WISH following *soxB1-*  
710 *2 RNAi*. (B-D) WISH for *pkd* genes on intact or 14 dpa *soxB1-2(RNAi)* regenerates that  
711 were amputated pre-pharyngeally. (B) Disrupting *soxB1-2* function in intact planarians  
712 led to reduced expression of *pkd* genes in the rheosensory organ (black arrows), the  
713 auricles, populations in the brain branches (black arrowheads), and in the dispersed  
714 subepidermal cells (inset images from dashed box areas). *pkd* expression appeared  
715 unaffected by *soxB1-2* RNAi in the pharynx and some brain branch populations as well  
716 as in the photoreceptors [see labeling in worms labeled with *pkd1L-1* (pharynx  
717 expression), *pkd1L-2* (photoreceptor expression), *pkd2-2* and *pkd2-3* (pharynx), *pkd2-4*  
718 (brain branch), and *pkd2L-2* (pharynx and brain branch)]. (C-D) *soxB1-2(RNAi)* head  
719 fragments that regenerated posterior tissues and new pharynx (C) or new heads (D)  
720 displayed loss of *pkd* labeling observed in intact planarians treated with dsRNA. Images  
721 cropped to display the regenerated tissues in each worm 14 dpa. Scale bars, 200 µm. n  
722 ≥ 3 worms tested, with all worms displaying similar expression patterns for all genes.  
723  
724

725 **Figure 4. Behavioral analysis reveals *pkd* genes involved in detecting**  
726 **mechanosensory stimulation.** (A-B) RNAi worms demonstrated significant reductions  
727 in their contraction behavior, represented as the percent change in length between pre-  
728 stimulus and post-stimulus worm length in vibration assays (see Figure S4 for the

729 schematic of RNAi and Assay) in both intact (A) and regenerate (B) RNAi worms. *pkd1L-*  
730 *2*, *pkd2-4*, and *pkd2L-1* RNAi results in decreased mechanosensation. Each worm  
731 assayed is represented as a dot on the graph; the boxes represent data ranges from the  
732 25<sup>th</sup> to the 75<sup>th</sup> percentile, with a bisecting line at the median and whiskers  
733 encompassing the full range of values for each experimental group. n ≥ 18 worms for  
734 each experimental group. \*\*\*\*p < 0.0001; all other groups are non-significant (p > 0.01);  
735 One-way ANOVA with Dunnett's multiple comparisons test.

736

737 **Figure 5. Feeding behavior analysis identifies candidate *pkd* genes implicated in**  
738 **chemosensation.** (A-B) A chemosensation assay was performed on intact and  
739 regenerated worms at 14 dpa. (A) The average total time (t) intact and regenerate  
740 planarians spent in the 'Food Zone' (a 10 mm region surrounding liver pellets in the test  
741 field) during the 10-minute assay period demonstrated a significant reduction in time  
742 spent in the food zone for *pkd2-4* worms (intact) and both *pkd1L-1* and *pkd2-4*  
743 regenerate worms. Animals that did not enter the food zone during the assay period  
744 were assigned a value of 0. (B) The percent of the worms in each experimental group  
745 that ate in the 10-minute assay period was calculated for both intact worms and  
746 regenerates, demonstrating significant reductions in the number of eating *pkd1L-*  
747 *1(RNAi)* and *pkd2-4(RNAi)* regenerated worms. The total number of worms used for the  
748 assay is displayed above the bars and applies to the data for both assays (A). \*\*p <  
749 0.01, \*\*\*p < 0.001, \*\*\*\*p < 0.0001, all other values were determined as not significant (p >  
750 0.01), One-way ANOVA with Dunnett's multiple comparisons test.

751

752 **Figure 6: *pkd* genes that produced RNAi phenotypes are co-expressed in sensory**  
753 **neurons.** (A-B) dFISH on *pkd1* genes (magenta) and *pkd2* genes (green) that resulted  
754 in behavioral phenotypes. (A) dFISH co-labeling of the two *pkd* genes that resulted in  
755 significant reductions in chemosensory behaviors, *pkd1L-1* and *pkd2-4*, shows that the  
756 more discrete population of *pkd1L-1* cells are co-labeled with *pkd2-4* in the auricle and  
757 brain branch region in both the ventral and dorsal regions of the head periphery  
758 (examples highlighted with white arrows). There are many additional *pkd2-4<sup>+</sup>* cells that  
759 were not co-labeled with *pkd1L-1* (examples highlighted with white arrowheads). (B)  
760 dFISH of the *pkd1* gene that resulted in a mechanosensory phenotype, *pkd1L-2*, with  
761 both of the *pkd2* genes that resulted in mechanosensory phenotypes, *pkd2L-2* and  
762 *pkd2-4*, showed that *pkd1L-2<sup>+</sup>* cells are co-expressed with both *pkd2* mechanosensory  
763 genes (examples highlighted with white arrows). *pkd2-4<sup>+</sup>* cells represent a larger  
764 population that also includes *pkd1L-2-* cells (examples highlighted with white  
765 arrowheads). White dashed boxes indicate the higher magnification image insets. Scale  
766 bars, 50 μm, n ≥ 3 worms tested with all worms displaying similar expression patterns.  
767

768 **Supplementary Material**

769 **Figure S1. A Bayesian inference phylogeny of PKD1 and PKD1L proteins.** Node  
770 support values are listed as percent support next to the relevant node.

771

772 **Figure S2. A Bayesian inference phylogeny of PKD2 proteins.** Node support values  
773 are listed as percent support next to the relevant node.

774

775 **Figure S3. In situ hybridization to *pkd* genes in *S. mediterranea* hermaphrodites.**

776 The expression of *pkd* genes mirrors in situ patterns in the asexual strain. However,  
777 eight out of nine planarian *pkd* genes (all except *pkd2L-2* in the bottom left panel)  
778 showed striking expression associated with reproductive structures: copulatory  
779 apparatus, ca; oviduct, od; gland cells, g; testes; and the gonopore, gn. Inset showed  
780 higher magnification of the copulatory apparatus regions for all genes detected. Scale  
781 bars = 500 µm.

782

783 **Figure S4. Timelines for RNAi experiments and vibration assay.** (A) Timeline for  
784 *pkd* RNAi experiments and subsequent behavioral testing. All testing was performed  
785 between 13- and 15-days following amputation. F, feed; D, day in an experiment; DPA,  
786 days post amputation. (C-E) depictions of the mechanosensory assays. (C) An  
787 illustration of the tapping device used to test mechanosensation is in Figure 4 (C'). A  
788 photo of the tapping device setup is shown. (D-E) Illustrations and still images from  
789 behavioral videos showing how pre-stimulus “gliding” length and post-stimulus  
790 “contraction” length were measured for the rheosensory (D) and vibration (E) assays.

791 The worms depicted are examples of a typical wild-type behavioral response. (F-G)  
792 Worms with *pkd* knockdowns that demonstrated a significant loss of mechanosensory  
793 function in the vibration assay were also tested using the rheosensory assay to validate  
794 the observed loss of mechanosensation in intact (F) and regenerate (G) worms. The  
795 percent change in length was calculated and plotted in a box plot wherein the box  
796 extends from the 25<sup>th</sup> to 75<sup>th</sup> percentiles of the range, and the bisecting line represents  
797 the median. The whiskers extend the full range of the data. *pkd1L-3*, which did not  
798 display a mechanosensory phenotype, was included as an additional negative control. n  
799 = 8-13 worms for each experimental group. \*\*\*p < 0.0001; all other groups are non-  
800 significant (p > 0.01); One-way ANOVA with Dunnett's multiple comparisons test.  
801

802 **Figure S5. Chemosensation assay.** (A) Illustration of the custom-made chamber used  
803 for chemosensation assays displaying the markings on the dish used to determine  
804 inclusion in the ‘feeding zone’ and start zone as explained in the methods. The lines  
805 were drawn on the bottom of the clear dish and could be visualized in the videos, which  
806 were taken with an overhead camera. (A') Photo of trays with drawn lines used in this  
807 study.  
808

809 **Table S1.** Results from BLAST of PKD domain to Planarian Transcriptome.  
810

811 **Table S2.** Primers and eBlock sequences used in this study.  
812

813 **File S1.** Protein sequences used for PKD1 phylogenetic analysis in Figure S1.

814

815 **File S2.** Protein sequences used for PKD2 phylogenetic analysis in Figure S1.

816

817 **File S3.** PKD1 cation channel alignment file used for phylogenetic analysis in Figure S1.

818

819 **File S4.** PKD2 cation channel alignment file used for phylogenetic analysis in Figure S2.

820

821 **File S5.** Link to Arduino code for controlling tapping device with servo motor

822

823 **Video S1.** Control worms 28 days following the first RNAi feeding display normal gliding

824 locomotion movements in the arena used for the chemosensory assay.

825

826 **Video S2.** *pkd2-4(RNAi)* worms 28 days following the first RNAi feeding display normal

827 gliding locomotion movements in the arena used for the chemosensory assay.

828

829 **Video S3.** Control worms at 55 days following the first RNAi feeding display normal

830 gliding locomotion movements.

831

832 **Video S4.** *pkd2-4(RNAi)* worms 55 days following the first RNAi feeding display slow,

833 inching, jerky locomotion movements.

834

835 **Tables**

836 **Table 1.** Summary of *Schmidtea mediterranea* PKD-like gene expression patterns,  
 837 regulation by *soxB1-2*, and RNAi phenotypes.

Gene Name	Dresden Transcript ID	Expression Pattern (Loss of expression observed after <i>soxB1-2</i> RNAi: Yes/No/Partial)							Observed Behavioral Phenotype
		BB	Aur	Brain	RO	DSC	PR	Ph	
<b>Pkd1 Family Members</b>									
<i>pkd1L-1</i>	dd_Smed_v6_15525_0_1	✓ (Y)				✓ (Y)		✓ (N)	Reduced chemosensory behaviors
<i>pkd1L-2</i>	dd_Smed_v6_13975_0_1				✓ (Y)		✓ (N)		Reduced mechanosensory behaviors
<i>pkd1L-3</i>	dd_Smed_v6_10962_0_1		✓ (Y)			✓ (Y)			None
<b>Pkd2 Family Members</b>									
<i>pkd2-1</i>	dd_Smed_v6_12955_0_1	✓ (Y)	✓ (Y)			✓ (Y)			None
<i>pkd2-2</i>	dd_Smed_v6_17348_0_3							✓ (N)	None
<i>pkd2-3</i>	dd_Smed_v6_17348_0_2							✓ (N)	None
<i>pkd2-4*</i>	dd_Smed_v6_13327_0_1	✓ (P)	✓ (Y)		✓ (Y)	✓ (Y)			D26-D40, 8-feed RNAi: Reduced chemosensory behaviors; Reduced mechanosensory behaviors
									Extended RNAi, D55, 8- and 14-feed RNAi: slow inching, jerky movements observed in Ross et al., 2018. (18/18 worms)
<i>pkd2L-1</i>	dd_Smed_v6_15626_0_1				✓ (Y)		✓ (**)		Reduced mechanosensory behaviors
<i>pkd2L-2</i>	dd_Smed_v6_9977_0_3	✓ (P)	✓ (Y)	✓ (N)		✓ (Y)		✓ (N)	None

838

839 Abbreviations: BB, Brain Branches; Aur, Auricles; RO, rheosensory organ (both the dorsal ciliated stripe  
 840 and dorsal and ventral peripheral ciliated stripes); DSC, Dispersed Subepidermal Cells; PR,  
 841 photoreceptors; Ph, pharynx; D, day; DPA, days post-amputation. \*The severity of movement defects  
 842 precluded quantification of behaviors for the extended RNAi. Videos of control and *pkd2-4(RNAi)* D28  
 843 (normal movement) and D55 (abnormal movements) shown in Videos S1-S4. \*\*Not scored.  
 844

## 845 References

- 846 Adler, C.E., and Alvarado, A.S. (2018). Systemic RNA Interference in Planarians by  
847 Feeding of dsRNA Containing Bacteria. *Methods Mol Biol* 1774, 445-454.
- 848 Allen, G.D. (1915). REVERSIBILITY OF THE REACTIONS OF PLANARIA  
849 DOROTOCEPHALA TO A CURRENT OF WATER. *The Biological Bulletin* 29,  
850 111-[128]-111.
- 851 Almazan, E.M.P., Ryan, J.F., and Rouhana, L. (2021). Regeneration of Planarian  
852 Auricles and Reestablishment of Chemotactic Ability. *Front Cell Dev Biol* 9,  
853 777951.
- 854 Arnold, C.P., Lozano, A.M., Mann, F.G., Jr., et al. (2021). Hox genes regulate asexual  
855 reproductive behavior and tissue segmentation in adult animals. *Nat Commun*  
856 12, 6706.
- 857 Barr, M.M., DeModena, J., Braun, D., et al. (2001). The *Caenorhabditis elegans*  
858 autosomal dominant polycystic kidney disease gene homologs *lov-1* and *pkd-2*  
859 act in the same pathway. *Curr Biol* 11, 1341-1346.
- 860 Edgar, R.C. (2022). Muscle5: High-accuracy alignment ensembles enable unbiased  
861 assessments of sequence homology and phylogeny. *Nat Commun* 13, 6968.
- 862 England, S.J., Campbell, P.C., Banerjee, S., et al. (2017). Identification and Expression  
863 Analysis of the Complete Family of Zebrafish *pkd* Genes. *Front Cell Dev Biol* 5,  
864 5.
- 865 Esarte Palomero, O., Larmore, M., and DeCaen, P.G. (2023). Polycystin Channel  
866 Complexes. *Annu Rev Physiol* 85, 425-448.
- 867 Farnesi, R.M., and Tei, S. (1980). *Dugesia lugubris* s.l. auricles: research into the  
868 ultrastructure and on the functional efficiency. *Riv Biol* 73, 65-77.
- 869 Fedele, S.V., Gallagher, A.R., and Somlo, S. (2014). Polycystin-1: a master regulator  
870 of intersecting cystic pathways. *Trends Mol Med* 20, 251-260.
- 871 Fincher, C.T., Wurtzel, O., de Hoog, T., et al. (2018). Cell type transcriptome atlas for  
872 the planarian *Schmidtea mediterranea*. *Science* 360.
- 873 Fraenkel, A., Gunn, D. L. (1961). The orientation of animals. New York: Dover.
- 874 Gao, Z., Ruden, D.M., and Lu, X. (2003). PKD2 cation channel is required for directional  
875 sperm movement and male fertility. *Curr Biol* 13, 2175-2178.
- 876 Grohme, M.A., Schloissnig, S., Rozanski, A., et al. (2018). The genome of *Schmidtea*  
877 *mediterranea* and the evolution of core cellular mechanisms. *Nature* 554, 56-61.

- 878 Harris, P.C., and Torres, V.E. (2009). Polycystic kidney disease. *Annu Rev Med* 60,  
879 321-337.
- 880 Horio, N., Yoshida, R., Yasumatsu, K., et al. (2011). Sour taste responses in mice  
881 lacking PKD channels. *PLoS One* 6, e20007.
- 882 Huelsenbeck, J.P., and Ronquist, F. (2001). MRBAYES: Bayesian inference of  
883 phylogenetic trees. *Bioinformatics* 17, 754-755.
- 884 Hulett, R.E., Gehrke, A.R., Gompers, A., et al. (2023). A wound-induced differentiation  
885 trajectory for neurons. *bioRxiv*.
- 886 Hulett, R.E., Rivera-Lopez, C., Gehrke, A.R., et al. (2024). A wound-induced  
887 differentiation trajectory for neurons. *Proc Natl Acad Sci U S A* 121,  
888 e2322864121.
- 889 Inoue, T., and Agata, K. (2022). Quantification of planarian behaviors. *Dev Growth  
890 Differ* 64, 16-37.
- 891 Inoue, T., Yamashita, T., and Agata, K. (2014). Thermosensory signaling by TRPM is  
892 processed by brain serotonergic neurons to produce planarian thermotaxis. *J  
893 Neurosci* 34, 15701-15714.
- 894 Ishimaru, Y., Inada, H., Kubota, M., et al. (2006). Transient receptor potential family  
895 members PKD1L3 and PKD2L1 form a candidate sour taste receptor. *Proc Natl  
896 Acad Sci U S A* 103, 12569-12574.
- 897 Issigonis, M., Browder, K.L., Chen, R., et al. (2024). A niche-derived nonribosomal  
898 peptide triggers planarian sexual development. *Proc Natl Acad Sci U S A* 121,  
899 e2321349121.
- 900 Issigonis, M., and Newmark, P.A. (2019). From worm to germ: Germ cell development  
901 and regeneration in planarians. *Curr Top Dev Biol* 135, 127-153.
- 902 Issigonis, M., Redkar, A.B., Rozario, T., et al. (2022). A Kruppel-like factor is required  
903 for development and regeneration of germline and yolk cells from somatic stem  
904 cells in planarians. *PLoS Biol* 20, e3001472.
- 905 Ivankovic, M., Haneckova, R., Thommen, A., et al. (2019). Model systems for  
906 regeneration: planarians. *Development* 146.
- 907 Kierszenbaum, A.L. (2004). Polycystins: what polycystic kidney disease tells us about  
908 sperm. *Mol Reprod Dev* 67, 385-388.
- 909 King, H.O., Owusu-Boaitey, K.E., Fincher, C.T., et al. (2024). A transcription factor atlas  
910 of stem cell fate in planarians. *Cell Rep* 43, 113843.

- 911 King, R.S., and Newmark, P.A. (2013). In situ hybridization protocol for enhanced  
912 detection of gene expression in the planarian *Schmidtea mediterranea*. BMC Dev  
913 Biol 13, 8.
- 914 Koehler, O. (1932). Beiträge zur Sinnesphysiologie der Süßwasserplanarien. Z. vergl.  
915 Physiol. 16, 606-756.
- 916 Liu, C., and Montell, C. (2015). Forcing open TRP channels: Mechanical gating as a  
917 unifying activation mechanism. Biochem Biophys Res Commun 460, 22-25.
- 918 LopezJimenez, N.D., Cavenagh, M.M., Sainz, E., et al. (2006). Two members of the  
919 TRPP family of ion channels, Pkd1l3 and Pkd2l1, are co-expressed in a subset of  
920 taste receptor cells. J Neurochem 98, 68-77.
- 921 Maser, R.L., Calvet, J.P., and Parnell, S.C. (2022). The GPCR properties of polycystin-  
922 1- A new paradigm. Front Mol Biosci 9, 1035507.
- 923 McLaughlin, S. (2017). Evidence that polycystins are involved in Hydra cnidocyte  
924 discharge. Invert Neurosci 17:1.
- 925 Miyamoto, M., Hattori, M., Hosoda, K., et al. (2020). The pharyngeal nervous system  
926 orchestrates feeding behavior in planarians. Sci Adv 6, eaaz0882.
- 927 Morris, Z., Sinha, D., Poddar, A., et al. (2019). Fission yeast TRP channel Pkd2p  
928 localizes to the cleavage furrow and regulates cell separation during cytokinesis.  
929 Mol Biol Cell 30, 1791-1804.
- 930 O'Hagan, R., Wang, J., and Barr, M.M. (2014). Mating behavior, male sensory cilia, and  
931 polycystins in *Caenorhabditis elegans*. Semin Cell Dev Biol 33, 25-33.
- 932 Ohata, S., Herranz-Perez, V., Nakatani, J., et al. (2015). Mechanosensory Genes Pkd1  
933 and Pkd2 Contribute to the Planar Polarization of Brain Ventricular Epithelium. J  
934 Neurosci 35, 11153-11168.
- 935 Pearson, B.J., Eisenhoffer, G.T., Gurley, K.A., et al. (2009). Formaldehyde-based  
936 whole-mount in situ hybridization method for planarians. Dev Dyn 238, 443-450.
- 937 Plass, M., Solana, J., Wolf, F.A., et al. (2018). Cell type atlas and lineage tree of a  
938 whole complex animal by single-cell transcriptomics. Science 360.
- 939 Reddien, P.W. (2018). The Cellular and Molecular Basis for Planarian Regeneration.  
940 Cell 175, 327-345.
- 941 Roberts-Galbraith, R.H., Brubacher, J.L., and Newmark, P.A. (2016). A functional  
942 genomics screen in planarians reveals regulators of whole-brain regeneration.  
943 Elife 5.

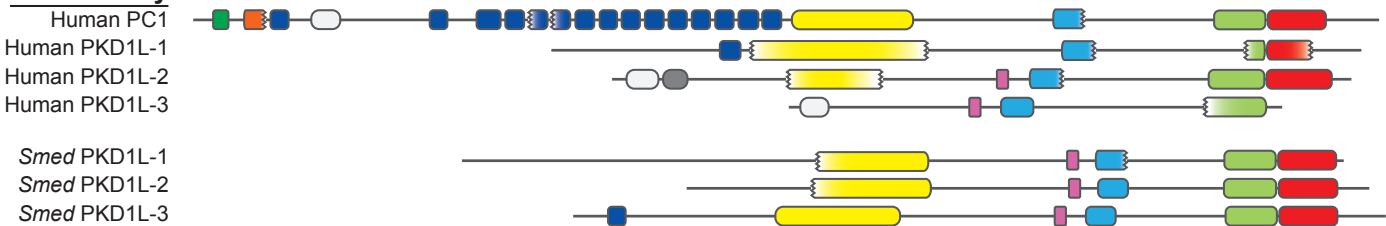
- 944 Ross, K.G., Currie, K.W., Pearson, B.J., et al. (2017). Nervous system development and  
945 regeneration in freshwater planarians. Wiley Interdiscip Rev Dev Biol 6.
- 946 Ross, K.G., Molinaro, A.M., Romero, C., et al. (2018). SoxB1 Activity Regulates  
947 Sensory Neuron Regeneration, Maintenance, and Function in Planarians. Dev  
948 Cell 47, 331-347 e335.
- 949 Rouhana, L., Weiss, J.A., Forsthöfel, D.J., et al. (2013). RNA interference by feeding in  
950 vitro-synthesized double-stranded RNA to planarians: methodology and  
951 dynamics. Dev Dyn 242, 718-730.
- 952 Rozanski, A., Moon, H., Brandl, H., et al. (2019). PlanMine 3.0-improvements to a  
953 mineable resource of flatworm biology and biodiversity. Nucleic Acids Res 47,  
954 D812-D820.
- 955 Sakagami, T., Watanabe, K., Hamada, M., et al. (2024). Structure of putative epidermal  
956 sensory receptors in an acoel flatworm, Praesagittifera naikaiensis. Cell Tissue  
957 Res 395, 299-311.
- 958 Schindelin, J., Arganda-Carreras, I., Frise, E., et al. (2012). Fiji: an open-source  
959 platform for biological-image analysis. Nat Methods 9, 676-682.
- 960 Sebe-Pedros, A., Saudemont, B., Chomsky, E., et al. (2018). Cnidarian Cell Type  
961 Diversity and Regulation Revealed by Whole-Organism Single-Cell RNA-Seq.  
962 Cell 173, 1520-1534 e1520.
- 963 Thi-Kim Vu, H., Rink, J.C., McKinney, S.A., et al. (2015). Stem cells and fluid flow drive  
964 cyst formation in an invertebrate excretory organ. Elife 4.
- 965 Van Goethem, E., Silva, E.A., Xiao, H., et al. (2012). The Drosophila TRPP cation  
966 channel, PKD2 and Dmel/Ced-12 act in genetically distinct pathways during  
967 apoptotic cell clearance. PLoS One 7, e31488.
- 968 Wang, J., Chitsaz, F., Derbyshire, M.K., et al. (2023). The conserved domain database  
969 in 2023. Nucleic Acids Res 51, D384-D388.
- 970 Watnick, T.J., Jin, Y., Matunis, E., et al. (2003). A flagellar polycystin-2 homolog  
971 required for male fertility in Drosophila. Curr Biol 13, 2179-2184.
- 972 Wurtzel, O., Cote, L.E., Poirier, A., et al. (2015). A Generic and Cell-Type-Specific  
973 Wound Response Precedes Regeneration in Planarians. Dev Cell 35, 632-645.  
974

975

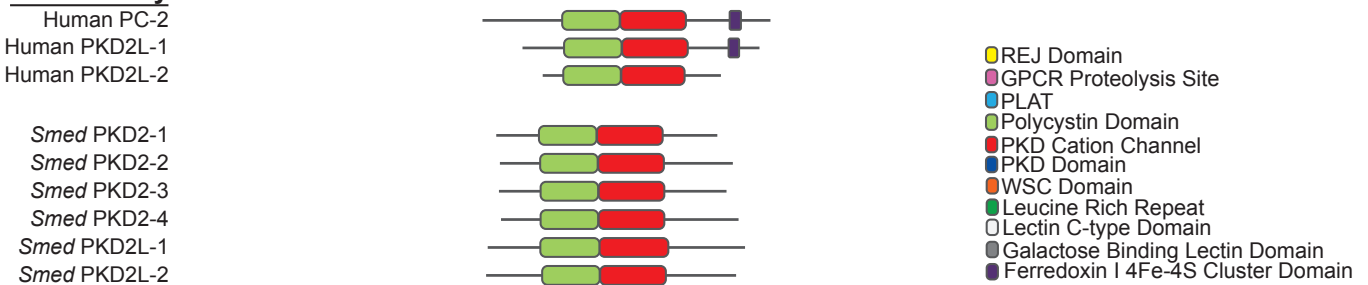
**Figure 1**

**A**

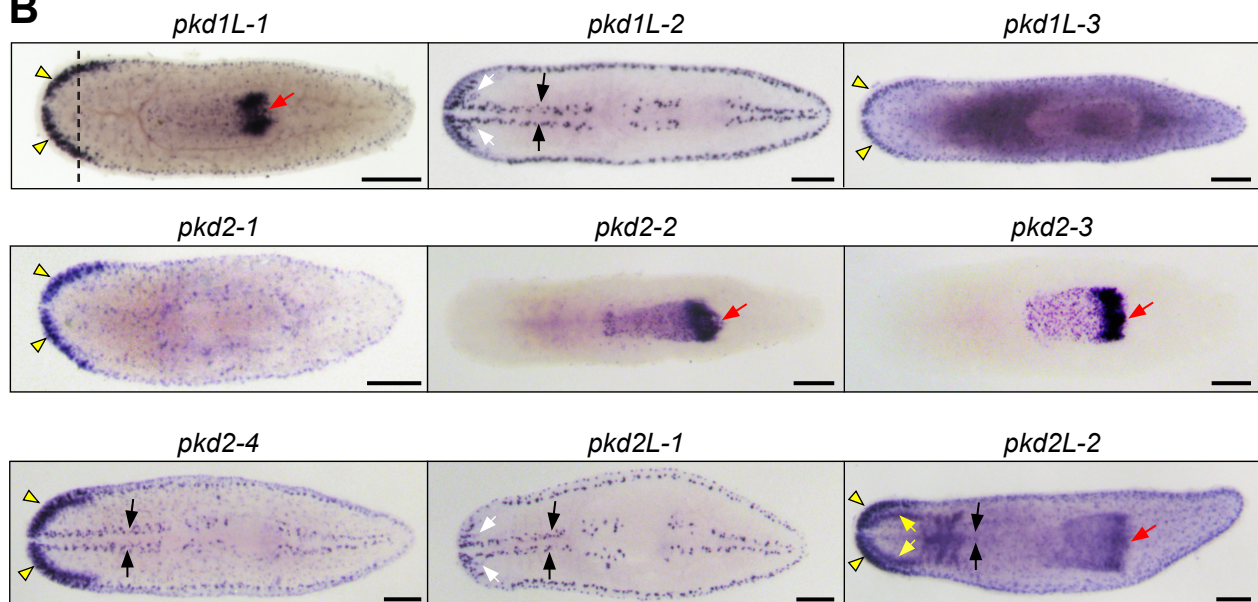
**PKD1 family**



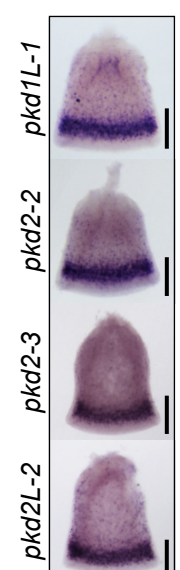
**PKD2 family**



**B**



**C**



**B'**

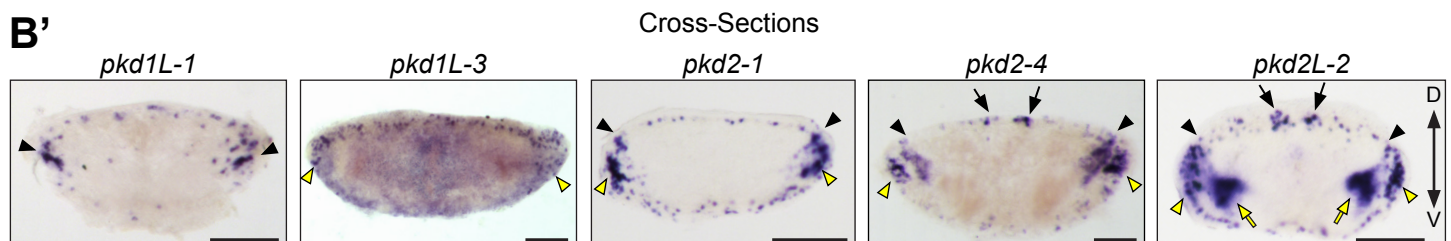


**Figure 2**

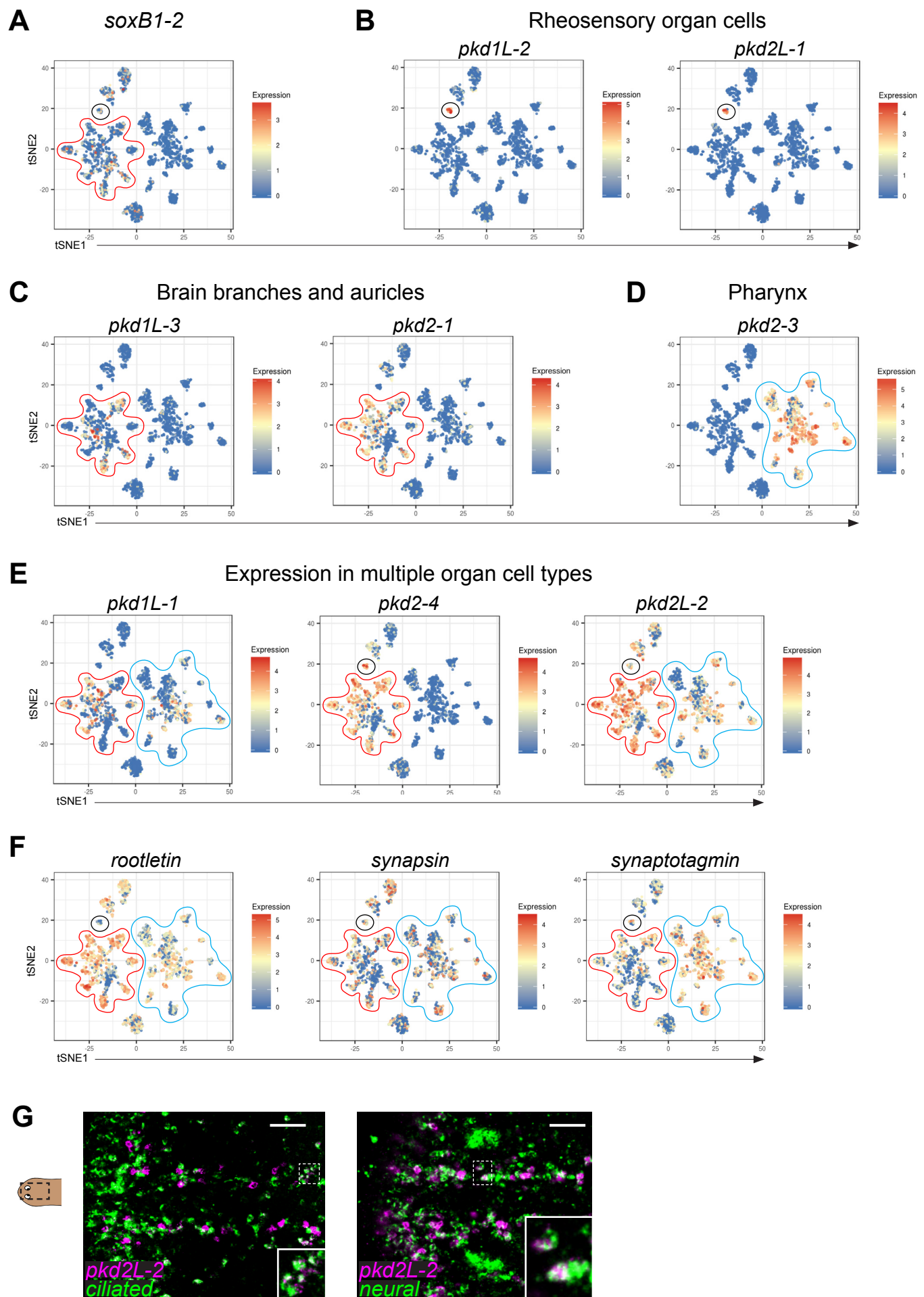
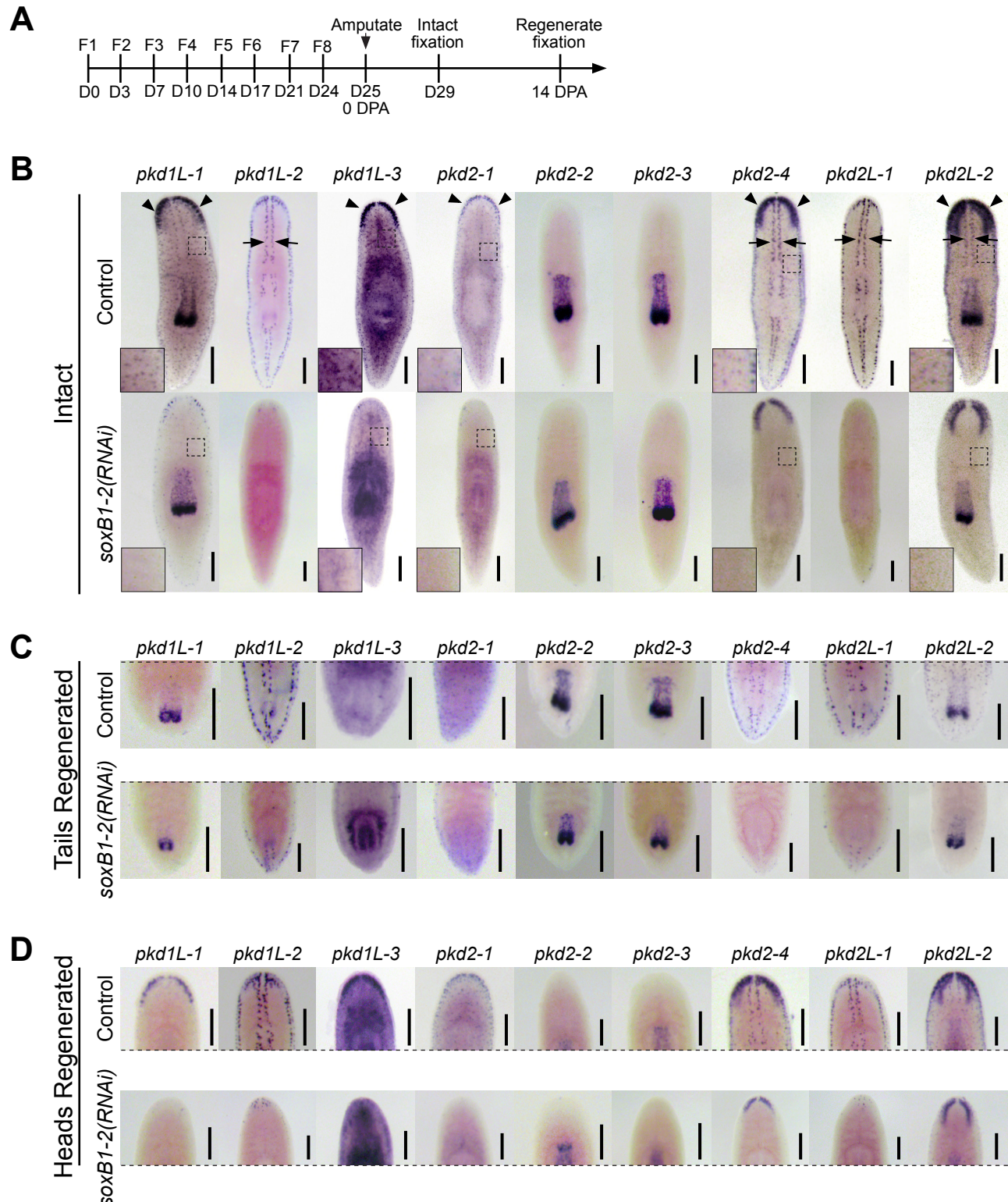


Figure 3



## Figure 4<sup>was</sup>

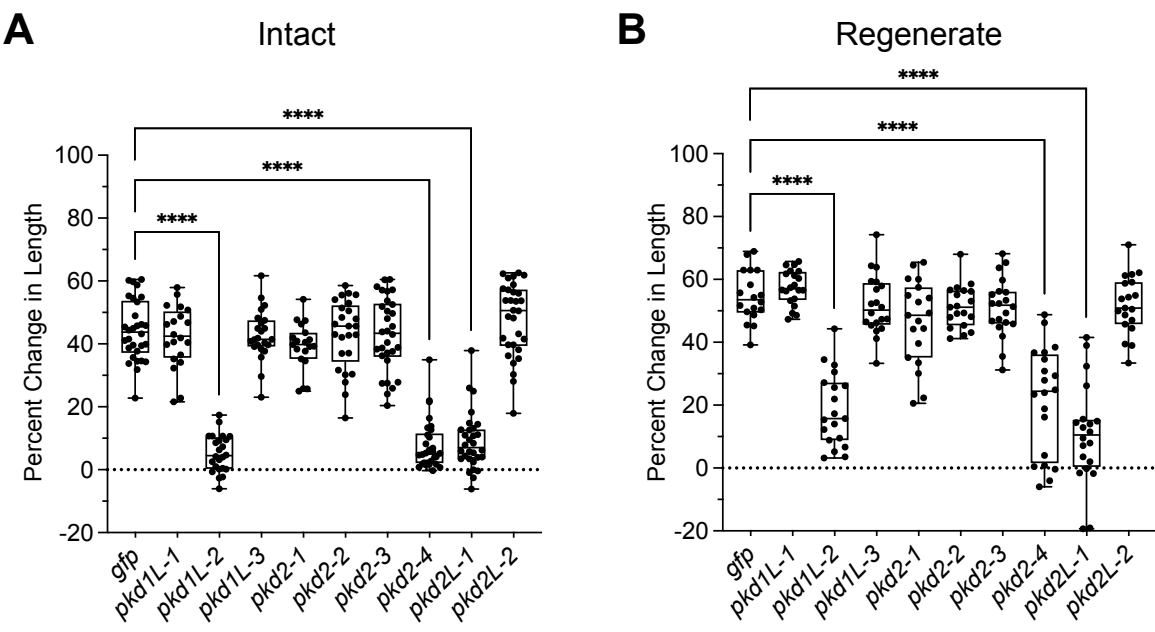


Figure 5

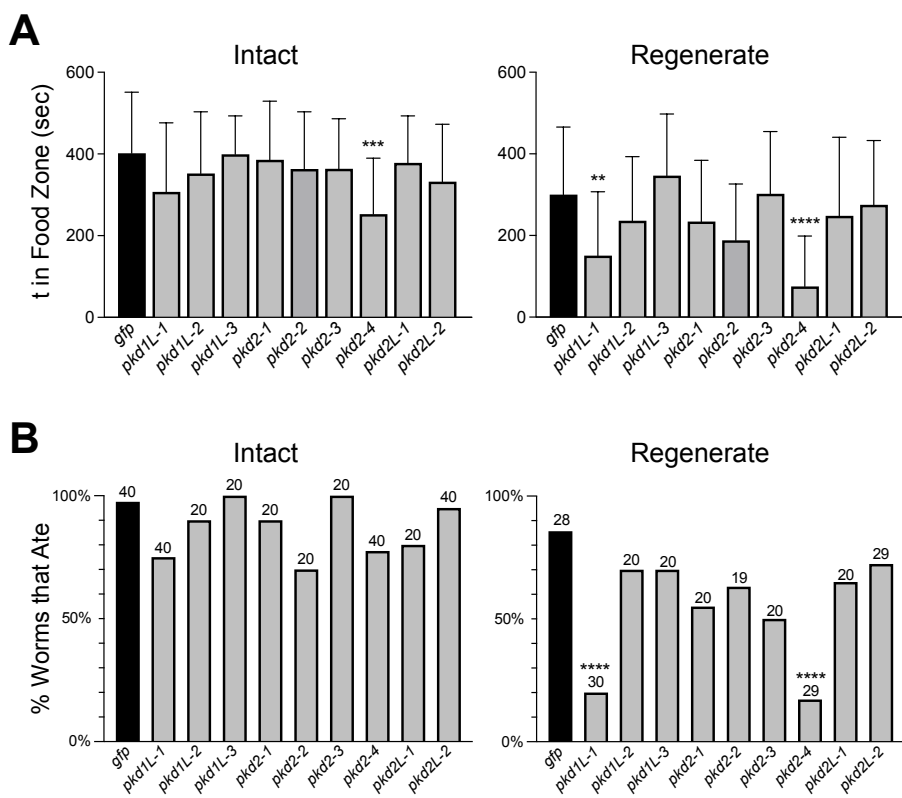
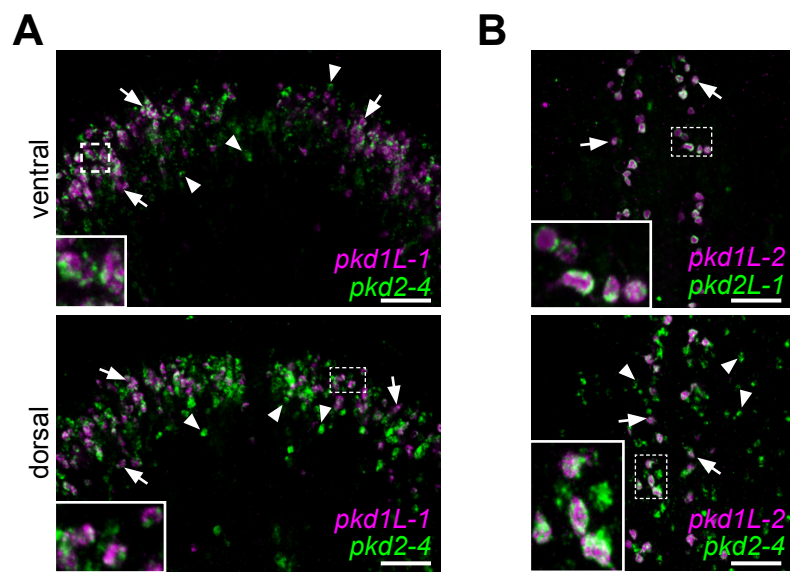
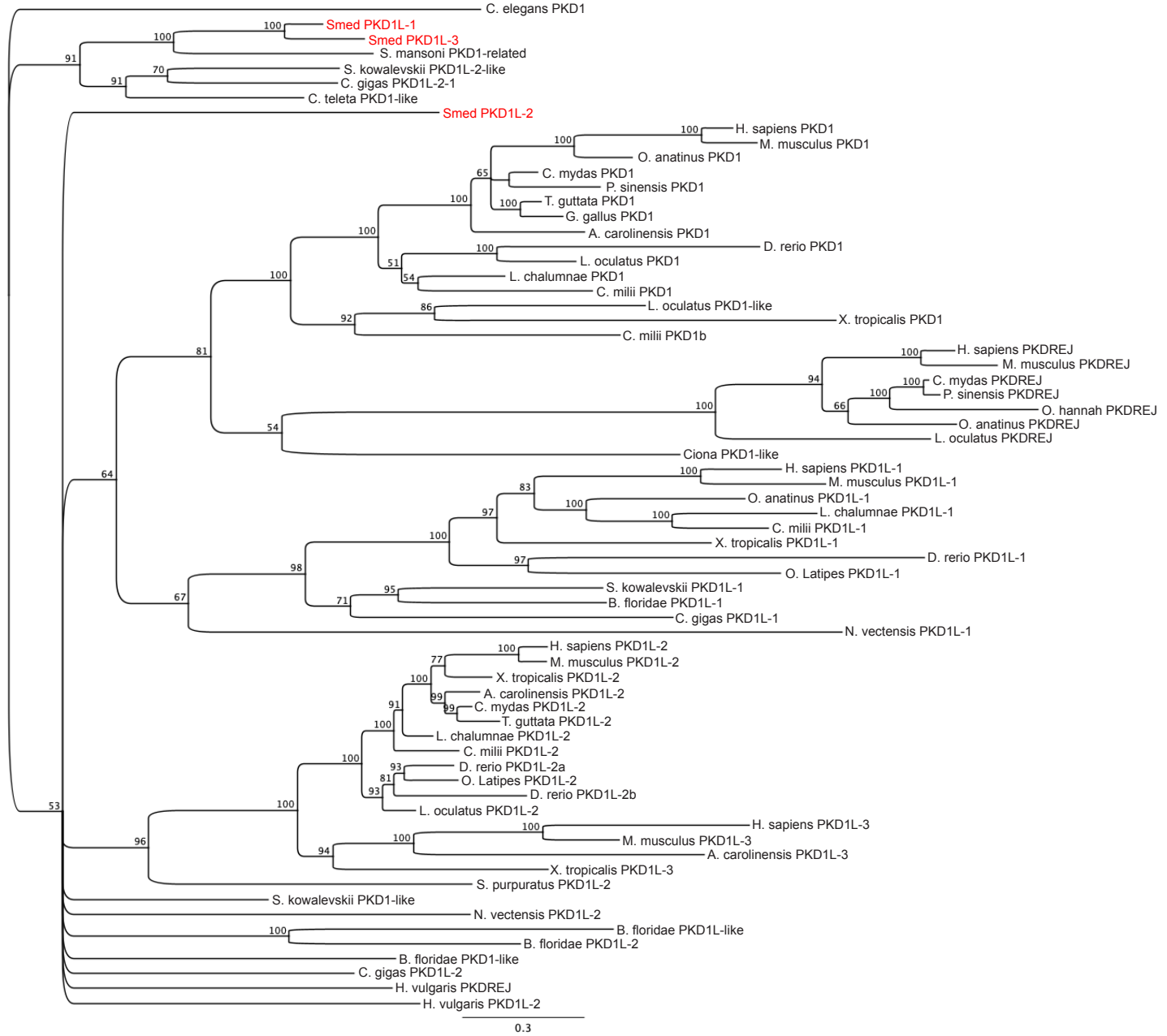


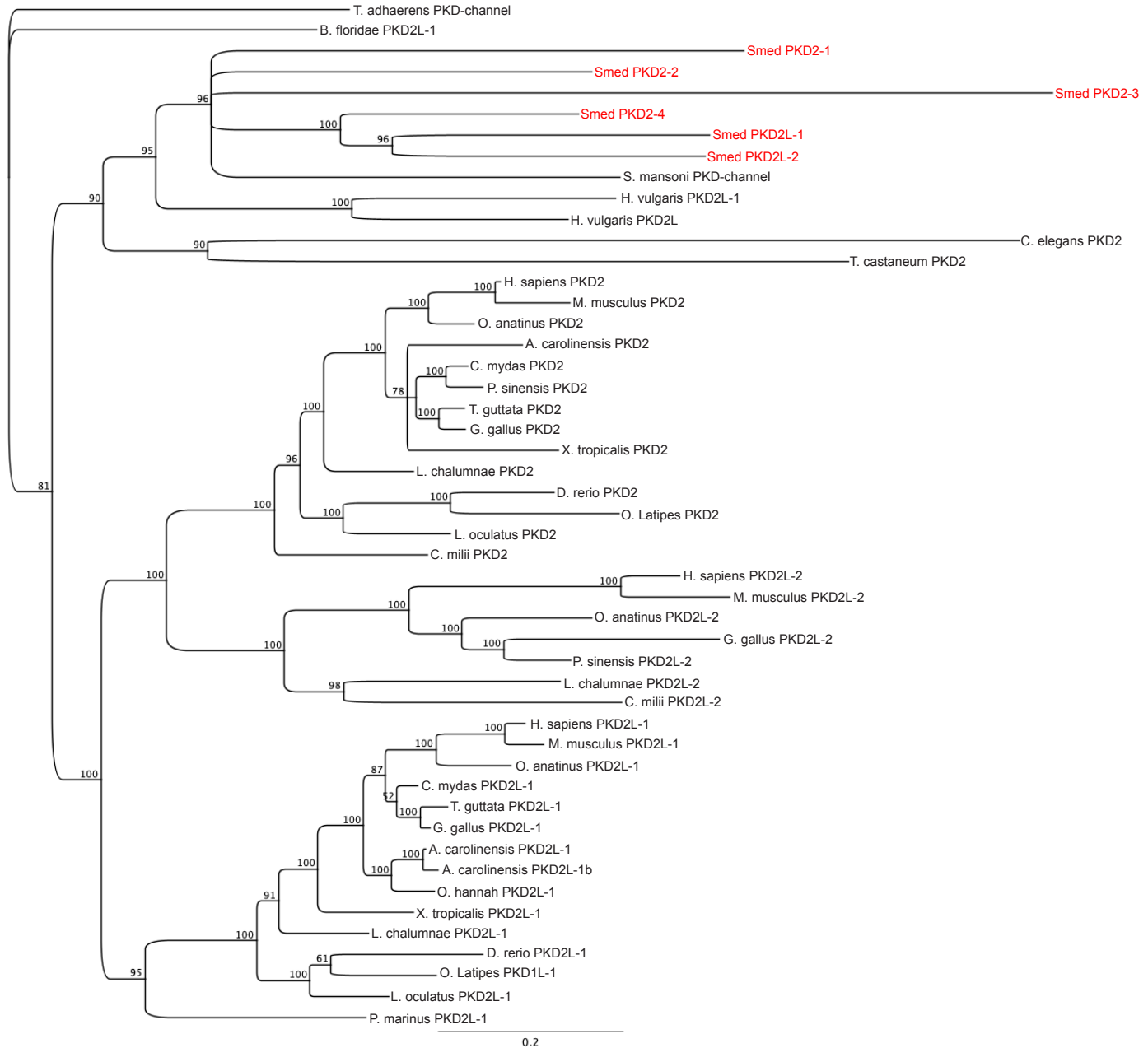
Figure 6



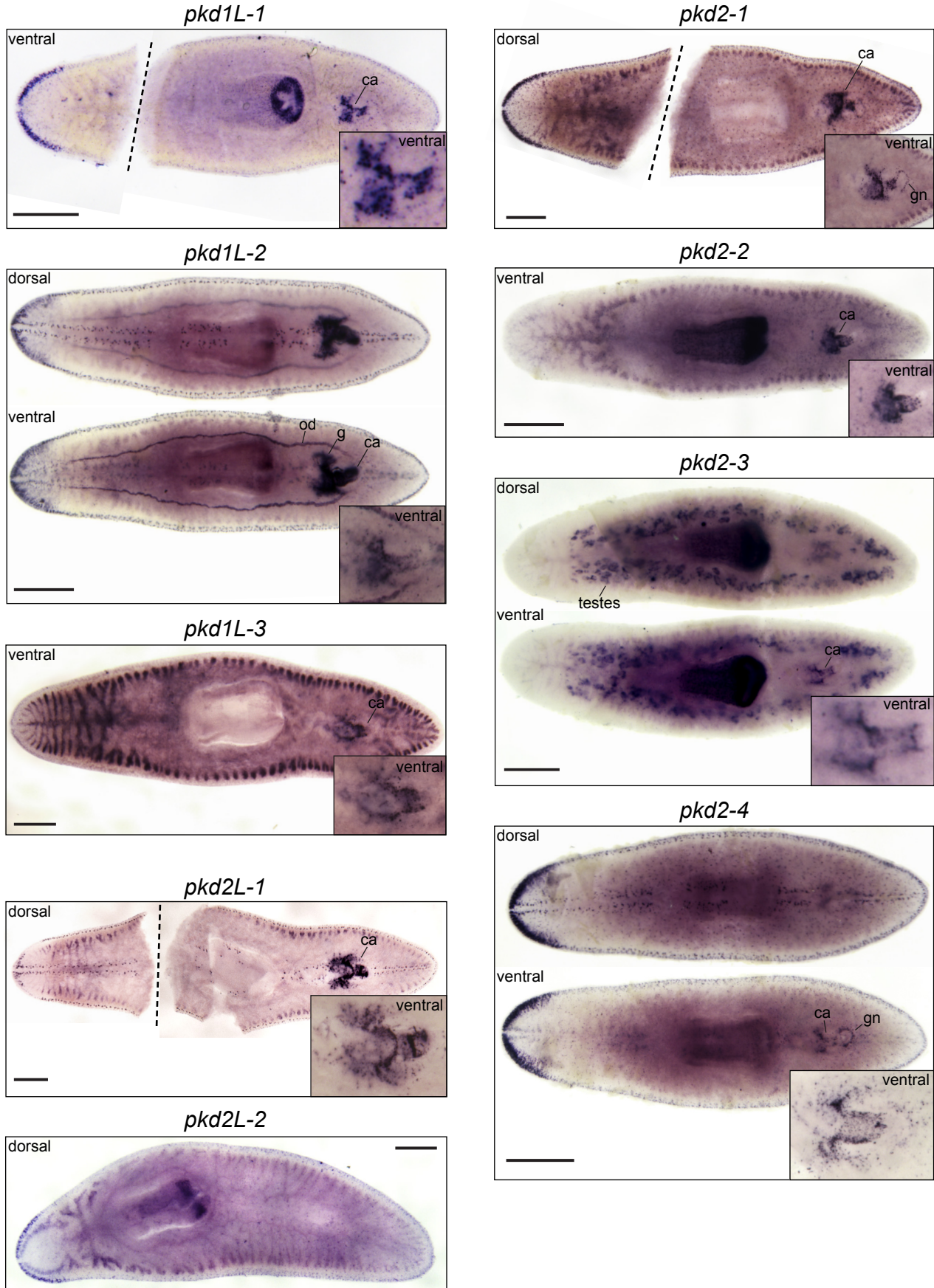
## Supplementary Figure 1



Supplementary Figure 2



Supplementary Figure 3

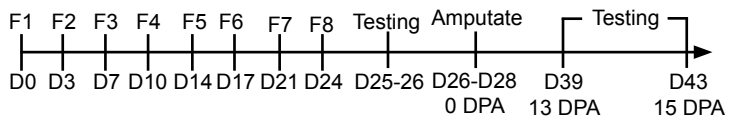


## Supplementary Figure 4

**A**

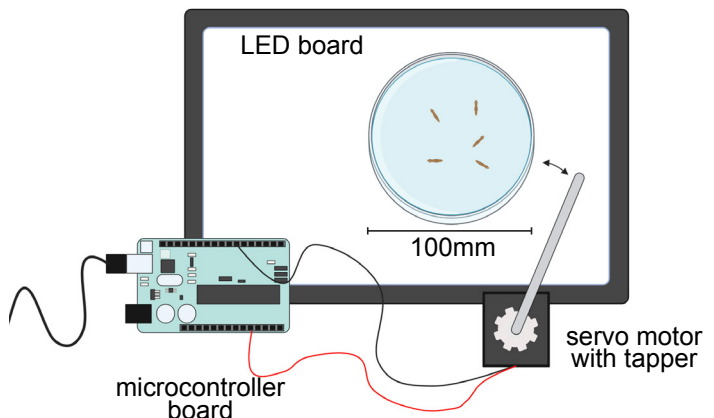


**B**

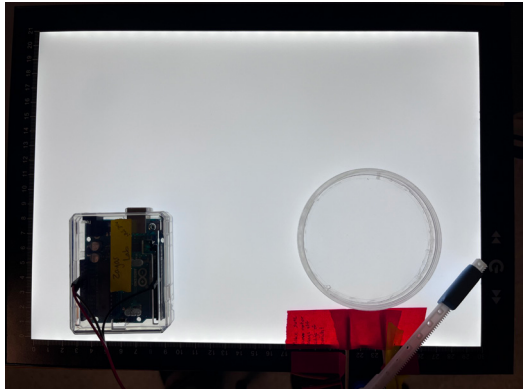


**C**

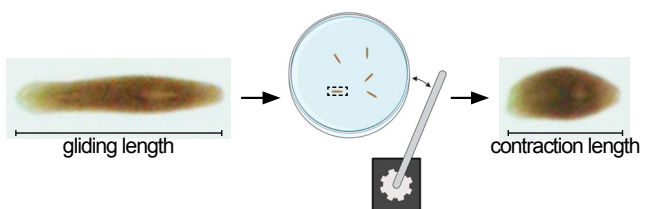
### Vibration Assay Set-Up



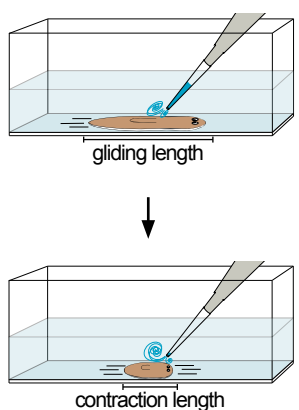
**C'**



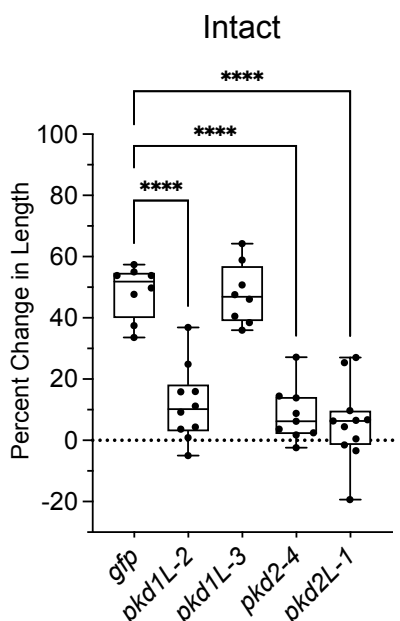
**D**



**E**

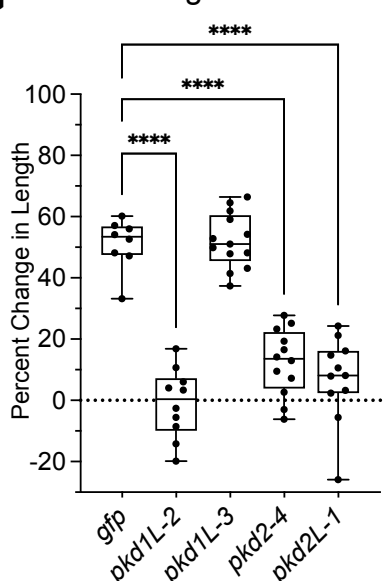


**F**



Intact

**G**

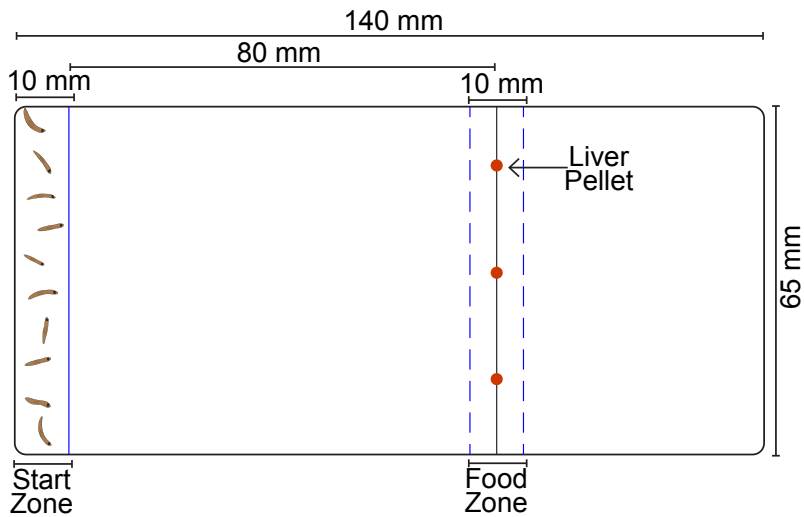


Regenerate

Supplementary Figure 5

### Chemosensation Assay Set-Up

A



A'

